Received: 1 June 2023 | Revised: 16 August 2023 | Accepted: 21 August 2023

DOI: 10.1002/gj.4872

RESEARCH ARTICLE

WILEY

A journey of the continental crust to and from mantle depth: The *P–T–t-d* path of Venaco unit, Alpine Corsica (France)

Maria Di Rosa[1] | E. Sanità[1] | C. Frassi[1] | J. M. Lardeaux[2,3] | M. Corsini[2,3] | M. Marroni[1,4] | L. Pandolfi[1]

[1]Dipartimento di Scienze della Terra, Università di Pisa, Pisa, Italy

[2]UMR, CNRS, Observatoire de la Côte d'Azur, Géoazur, Université Côte d'Azur, Valbonne, France

[3]Centre for Lithospheric Reseach, Czech Geological Survey, Prague, Czech Republic

[4]Consiglio Nazionale della Ricerca, Istituto di Geoscienze e Georisorse, IGG-CNR, Pisa, Italy

Correspondence
Maria Di Rosa, Dipartimento di Scienze della Terra, Università di Pisa, Via Santa Maria, 53, Pisa, Italy.
Email: maria.dirosa@unipi.it

Funding information
PRA Project Meneghini 2022

Handling Editor: I. D. Somerville

This work presents the first pressure–temperature-deformation-time (*P–T-d-t*) path obtained for the Lower Units (Alpine Corsica, France) including the Tenda Massif that represent fragments of the European continental margin involved in the east-dipping Alpine subduction. The new thermobarometric data applied to metapelites and the new $^{40}Ar/^{39}Ar$ dating of syn-kinematic muscovite sampled from metagranitoids allowed us to define the *P–T* conditions and the age of the metamorphism of the Venaco Unit, a Lower Unit located in the southernmost sector of the Alpine Corsica. The outcoming scenario indicates that the Venaco Unit reached the baric peak at ≈ 33 km depth, not before Bartonian time. At 35.7 Ma (i.e., during the middle Priabonian), it was exhumed to a shallower structural level (i.e., at ≈ 26 km depth), mainly through the activation of the top-to-W shear zones. This retrograde path suggests that the Venaco Unit experienced fast exhumation, unlike the Tenda Massif which had been involved in subduction during the Ypresian and was stationary at 25–30 km, before its exhumation in the Priabonian.

KEYWORDS
Alpine Orogeny, blueschist-facies metamorphism, cold vs. warm exhumation path, European continental unit, Lower Units (Alpine Corsica)

1 | INTRODUCTION

Tectono-metamorphic investigation on deformed rocks helps to constrain the evolution of collisional belts. Modelling pressure (*P*) and temperature (*T*) conditions through time (*t*) and within a deformation (*d*) frame (*P–T-d-t* path) of oceanic and continental tectonic units allow to individualize the events of the oceanic/continental subduction, continental collision and the subsequent progressive exhumation that characterize the evolution of worldwide collisional belts. Because of their ability to bind the history of tectonic units in space and time, *P–T-d-t* paths have achieved a great success over the past 30 years in the study of metamorphic rocks (e.g., Spear, 1993). One of the most investigated collisional belts is represented by the Alpine belt, where the study of rocks recording a wide range of deformation regimes and metamorphic conditions that helped to highlight the geodynamic evolution of this belt (e.g., Bousquet et al., 2008; Handy et al., 2010; Lardeaux & Spalla, 1991).

The Alpine Corsica (France) is interpreted as the southern branch of the Western Alps (Durand-Delga, 1984; Marroni & Pandolfi, 2003; Mattauer et al., 1981; Molli & Malavieille, 2011). It is a tectonic stack of tectono-metamorphic units with oceanic- and continental-affinities experiencing blueschist-eclogite to very low-grade facies metamorphic conditions during Late Cretaceous–early Oligocene subduction and continental collision-related processes (Elter & Pertusati, 1973; Lagabrielle & Polino, 1988; Malavieille et al., 1998; Michard & Martinotti, 2002; Molli, 2008; Schmid et al., 1996). Several slices with

continental affinity, known as Lower Units, experienced blueschist-facies metamorphism (Bezert & Caby, 1988; Di Rosa, De Giorgi, Marroni, & Vidal, 2017; Maggi et al., 2012; Malasoma & Marroni, 2007; Molli, 2008). They were deeply investigated because their tectono-metamorphic evolution provided useful information on the continental subduction stage (i.e., the transition between subduction and collision stages). Even if their *P–T* paths were obtained by several authors (Di Rosa, Frassi, et al., 2019; Frassi et al., 2022; Malasoma & Marroni, 2007; Molli et al., 2006), no age constraints on the metamorphic events are so far available.

In this work, we present a multidisciplinary dataset that includes micro- to meso-structural data, thermo-baric estimates, and muscovite $^{40}Ar/^{39}Ar$ single grain dating from one of the southernmost slices belonging to the Lower Units. The result is the first Pressure–Temperature-deformation-time (*P–T-d-t*) path for the continental units exposed at the western rim of the Alpine Corsica (i.e., External Continental Units, Figure 1). We discuss these new data to provide a new geodynamic reconstruction of the Alpine collisional belt.

2 | GEOLOGICAL SETTING

Corsica Island includes two geological domains, the so-called Hercynian and Alpine Corsica, exposed in the south-west and north-east portions of the island, respectively (Figure 1). The Hercynian Corsica consists of a polymetamorphic basement recording Pan-African and Variscan orogenic events intruded by Permo-Carboniferous magmatic rocks (Cabanis et al., 1990; Laporte et al., 1991; Ménot & Orsini, 1990; Paquette et al., 2003; Rossi et al., 2009; Rossi et al., 2015). This basement is covered by sedimentary successions including, Permian volcaniclastic and Mesozoic, mainly carbonates, unconformably covered by middle to late Eocene siliciclastic turbidites (Di Rosa, Frassi, Marroni, et al., 2020; Durand-Delga, 1984; Ferrandini et al., 2010; Rossi et al., 1994). The Hercynian Corsica is interpreted as the European continental margin that escaped from the Alpine Orogeny (e.g., Durand-Delga, 1984). The presence of localized shear zones of Tertiary ages affecting the late-Variscan magmatic suite (Di Vincenzo et al., 2016), and Eocene siliciclastic turbidites achieving blueschist metamorphic conditions (Di Rosa, 2021; Di Rosa, Frassi, Marroni, et al., 2020), however, in contrast with this original interpretation and demonstrate that the easternmost rim of Hercynian Corsica was instead involved in the Alpine Orogeny.

The Alpine Corsica consists of a stack of continental-, transitional- and oceanic-affinity units strongly deformed and affected by Cretaceous to Tertiary pervasive deformation and metamorphism, ranging from sub-greenschist to blueschist-eclogite facies (e.g., Gibbons & Horak, 1984; Malavieille et al., 1998; Marroni & Pandolfi, 2003; Mattauer et al., 1981; Vitale Brovarone et al., 2012). The Alpine Corsica overthrusts the Hercynian domain through an NNW–SSE trending, high-angle dipping thrust that runs across the entire island (e.g., Durand-Delga, 1984) (Figure 1).

The architecture of the Alpine Corsica mainly results from the convergence-related processes which started since the Late Cretaceous that initially produced the closure of an oceanic basin (i.e., the Liguro-Piemontese Basin) that opened between the Europe and Adria margins during Middle to Late Jurassic (Bill et al., 1997; Favre & Stampfli, 1992; Froitzheim & Manatchal, 1996; Manatschal, 1995; Marroni & Pandolfi, 2007). The convergence-related processes produced an east-dipping subduction of the oceanic lithosphere below the Adria Plate and the consequent Alpine accretionary. The progressive subduction of oceanic lithosphere led to the closure of the Liguro-Piemontese oceanic basin and the consequent collision between the European continental margin and the Alpine orogenic wedge during the middle Eocene-early Oligocene (Bezert & Caby, 1988; Di Rosa, Meneghini, Marroni, et al., 2020; Maggi et al., 2012; Malasoma et al., 2006; Mattauer & Proust, 1976). Simultaneously, the Ligure-Piemontese oceanic lithosphere that had not yet been involved in underthrusting, started to subduct toward the west below the European margin (Agard, 2021). This drastic change in the geodynamic scenario resulted in the large-scale extension of Alpine Corsica that produced the collapse and thermal re-equilibration of the previously thickened Alpine orogenic wedge and the consequent opening of two back-arc basins (i.e., the Liguro-Provençal and the Tyrrhenian Sea basins) that separated the Corsica-Sardinia continental microplate from the neighbouring domains of the Alpine and Apennine collisional belt, respectively (Daniel et al., 1996; Fournier et al., 1991; Jakni et al., 2000; Jolivet et al., 1991; Zarki-Jakni et al., 2004). Apatite fission track ages (≈ 23 Ma) obtained by Danišik et al. (2007) might support this thermal re-equilibration event (Di Rosa, Frassi, Marroni, et al., 2020).

The Alpine Corsica can be subdivided, from top to bottom (Figure 1) into: the Upper Units, the Schistes Lustrés Complex and the Lower Units. The Lower Units and the Schistes Lustrés Complex preserve a record of the subduction process. The Upper Units include slices of oceanic lithosphere characterized by very low-grade metamorphism achieved during their involvement in the subduction simultaneously to the Schistes Lustrés Complex but at a higher structural level (Durand-Delga et al., 1997; Marroni & Pandolfi, 2003; Pandolfi et al., 2016; Saccani et al., 2000). The Schistes Lustrés Complex is composed of oceanic and transitional units with high pressure-low temperature (*HP-LT*) metamorphic imprint (e.g., Guieu et al., 1994; Levi et al., 2007; Meresse et al., 2012; Ravna et al., 2010; Warburton, 1986), ranging in age between early and late Eocene (Brunet et al., 2000; Lahondère & Guerrot, 1997; Maluski, 1977; Martin et al., 2011; Vitale Brovarone & Herwartz, 2013). The Lower Units consist of continental crust slices derived from the thinned European margin involved in the subduction and accreted to the orogenic wedge. They include all the continental slices located along the western boundary of the Alpine Corsica (i.e., the External Continental Units of Malasoma & Marroni, 2007 and references therein) and the Tenda Massif, which is located east of the Balagne nappe (Figure 1). They show the same stratigraphic succession of the Hercynian Corsica, but in contrast, they are affected by blueschist-facies metamorphism (e.g., Di Rosa, Meneghini, et al., 2019; Gueydan et al., 2003; Malasoma & Marroni, 2007; Molli et al., 2006; Tribuzio & Giacomini, 2002) and by a polyphase deformation history with three ductile events

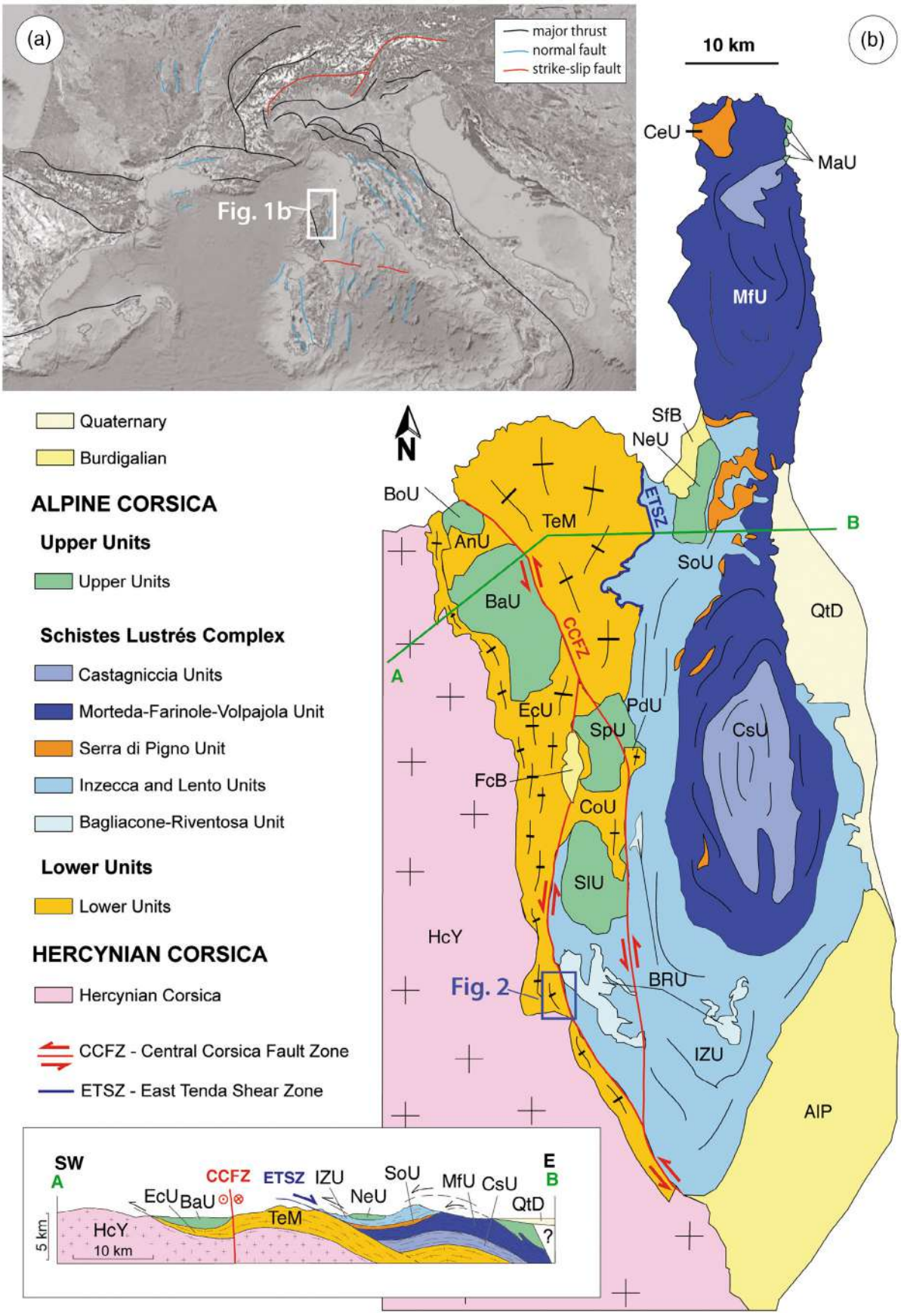

FIGURE 1 Legend on next page.

(Bezert & Caby, 1988; Bezert & Caby, 1989; Di Rosa, Frassi, et al., 2019; Garfagnoli et al., 2009; Malasoma & Marroni, 2007), achieved during the beginning of the exhumation (D1 phase), the exhumation within the subduction channel (D2 phase), and the final emplacement at shallower crustal levels in the extensional setting induced by the orogenic collapse (D3 phase). The depositional age of the Alpine foredeep deposits (breccias and sandstones) on the European continental margin is constrained to Lutetian-Priabonian (*Nummulites* sp., Amaudric du Chaffaut et al., 1985; Bezert & Caby, 1988; Di Rosa, De Giorgi, Marroni, & Vidal, 2017; Ferrandini et al., 2010). The age of the *HP-LT* metamorphism achieved by the European-affinity continental units was constrained only for the Tenda Massif, where Maggi et al. (2012) and Brunet et al. (2000) detected early to late Eocene ages. Similar ages were obtained for the shear zones located within the Hercynian Corsica (e.g., Razzo Bianco area) by Di Vincenzo et al. (2016).

After the D3 phase, a sinistral strike-slip fault system (i.e., Central Corsica Fault Zone–CCFZ of Waters, 1990; Ostriconi Fault of Lacombe & Jolivet, 2005) (Figure 1) cut both the stack of the Alpine Corsica and its western boundary with the Hercynian domain. The CCFZ is an important north–south-trending regional-scale structure (Di Rosa, De Giorgi, Marroni, & Pandolfi, 2017; Frassi et al., 2022; Lacombe & Jolivet, 2005; Malasoma et al., 2020; Maluski et al., 1973) stretching from the north, where it bounds the western side of the Tenda Massif, toward the south, where it splits in two branches in correspondence of the Asco valley (Figures 1 and 2, Di Rosa, 2021). Although there is no radiometric dating available to constrain the CCFZ activity, its activity can constrained by the age of the youngest deposits deformed by faults (i.e., the Lutetian-Priabonian foredeep deposits), and by the oldest deposits sealing the CCFZ structures (i.e., the Burdigalian-Langhian deposits of the Francardo basin; Alessandri et al., 1977; Ferrandini et al., 1998; Malasoma et al., 2020).

3 | METHODS

The techniques used in this work are: (1) structural mapping and mesoscale structural analysis, (2) microtectonic study of metagranitoids and metavolcaniclastics, (3) thermobarometry applied on metavolcaniclastics and metagranitoids and (4) $^{40}Ar/^{39}Ar$ dating of metamorphic white micas. Mineral chemistry of chlorite and phengite were performed with the electron probe microanalyser (EPMA) JEOL 8200 of the Università di Milano Statale "A. Desio", equipped with five wavelength-dispersive spectrometers. The point analyses were acquired using 15 KeV accelerating voltage, 5 nA specimen current and 30 s of dwell time for peaks and 10 s for background. Chlorite and phengite structural formulas were calculated assuming 14 and 11 anhydrous oxygens, respectively (Table 1).

Thermobarometry was performed on metapelites sampled in the metavolcaniclastics and metagranitoids. For metapelites, *P–T* equilibrium conditions of chlorite-phengite couples related to the D1 and D2 phases were estimated with the ChlMicaEqui software (Lanari, 2012) based on the Vidal and Parra (2000) method (Data S1). The results were compared with other thermometers (Bourdelle & Cathelineau, 2015; Cathelineau, 1988) and barometers (Bousquet et al., 2002; Dubacq et al., 2010). Thermobarometry on metagranitoids was performed using classical calibrations of Massonne and Schreyer (1987), Cathelineau (1988) and Cathelineau and Nieva (1985). Metamorphic white micas related to the D2 phase were separated from three samples of metagranitoids at the Dipartimento di Scienze della Terra (Università di Pisa) and hand-picked in CNRS (Géoazur, Valbonne). The analytical procedures and raw data are listed in the Appendix S1.

As regards the Ar/Ar dating, we analysed single muscovite grains by step heating. Sample CMD101 was crushed and 200–315 μm size fraction was cleaned in ultrasonic bath. Muscovite grains were carefully handpicked under a binocular microscope to select only grains without evidence of alteration or inclusions. Selected grains were packaged in aluminium foils and were irradiated for 97 h in the McMaster Nuclear Reactor (McMaster University, Ontario) together with Fish Canyon sanidine grains as flux monitor (28.030 ± 0.056 Ma, Jourdan & Renne, 2007). The argon isotopic interferences on K and Ca were determined by the irradiation of KF and CaF2 pure salts from which the following correction factors were obtained: $(^{40}Ar/^{39}Ar)K = 2.97 \times 10{-}2 \pm 10{-}3$ at 1S, $(^{38}Ar/^{39}Ar)K = 1.24 \times 10{-}2 \pm 5 \times 10{-}4$ at 1S, $(^{39}Ar/^{37}Ar)Ca = 7.27 \times 10{-}4 \pm 4 \times 10{-}5$ at 1S, and $(^{36}Ar/^{37}Ar)Ca = 2.82 \times 10{-}4 \pm 3 \times 10{-}5$ at 1S. $^{40}Ar/^{39}Ar$ step heating analyses were performed at Géoazur Nice (France) using a continuous 100 W PhotonMachine CO2 (IR) laser used at 5%–15% during 30 s. Argon isotopes were measured in static mode using an ARGUS VI mass spectrometer from ThermoFischer. Measurements were carried out in multi-collection mode using four Faraday cups equipped with 1012 ohm (masses 40, 39, 38 and 37) and one low-background compact discrete dynode ion counter to measure mass 36. Collector gain calibration is performed by the computer-controlled application of predetermined voltages to each collector. Mass discrimination for the mass spectrometer was monitored by regularly analysing air pipette volumes. The raw data (Data S1) were processed using the ArArCALC software (Koppers, 2002), and ages were calculated

FIGURE 1 (a) Localization of the study area into the western Mediterranean Sea; (b) tectonic map of north-eastern Corsica (modified after Di Rosa, Meneghini, Marroni, et al., 2020) and schematic cross-section (after Di Rosa, De Giorgi, Marroni, & Vidal, 2017). AlP, Aleria Plain; AnU, Annunciata Unit; BaU, Balagne Unit; BoU, Bas-Ostriconi Unit; BrU, Bagliacone- Riventosa Unit; CeU, Centuri Unit; CoU, Caporalino Unit; CsU, Castagniccia Unit; EcU, External Continental Units; cB, Francardo Basin; HcY, Hercynian Corsica; IZU, Inzecca and Lento Units; MaU, Macinaggio Unit; MfU, Morteda-Farinole-Volpajola Unit, Nebbio Unit; NeU, Neighbourhood Energy Utility; PdU, Cima Pedani Units; QtD. Quaternary deposits; SfB, Saint-Florent Basin; SlU, Santa Lucia Unit; SoU, Serra di Pigno and Oletta Units; SpU, Serra Debbione and Pineto Units; TeM, Tenda Massif. The location of the study area is marked by a blue rectangle.

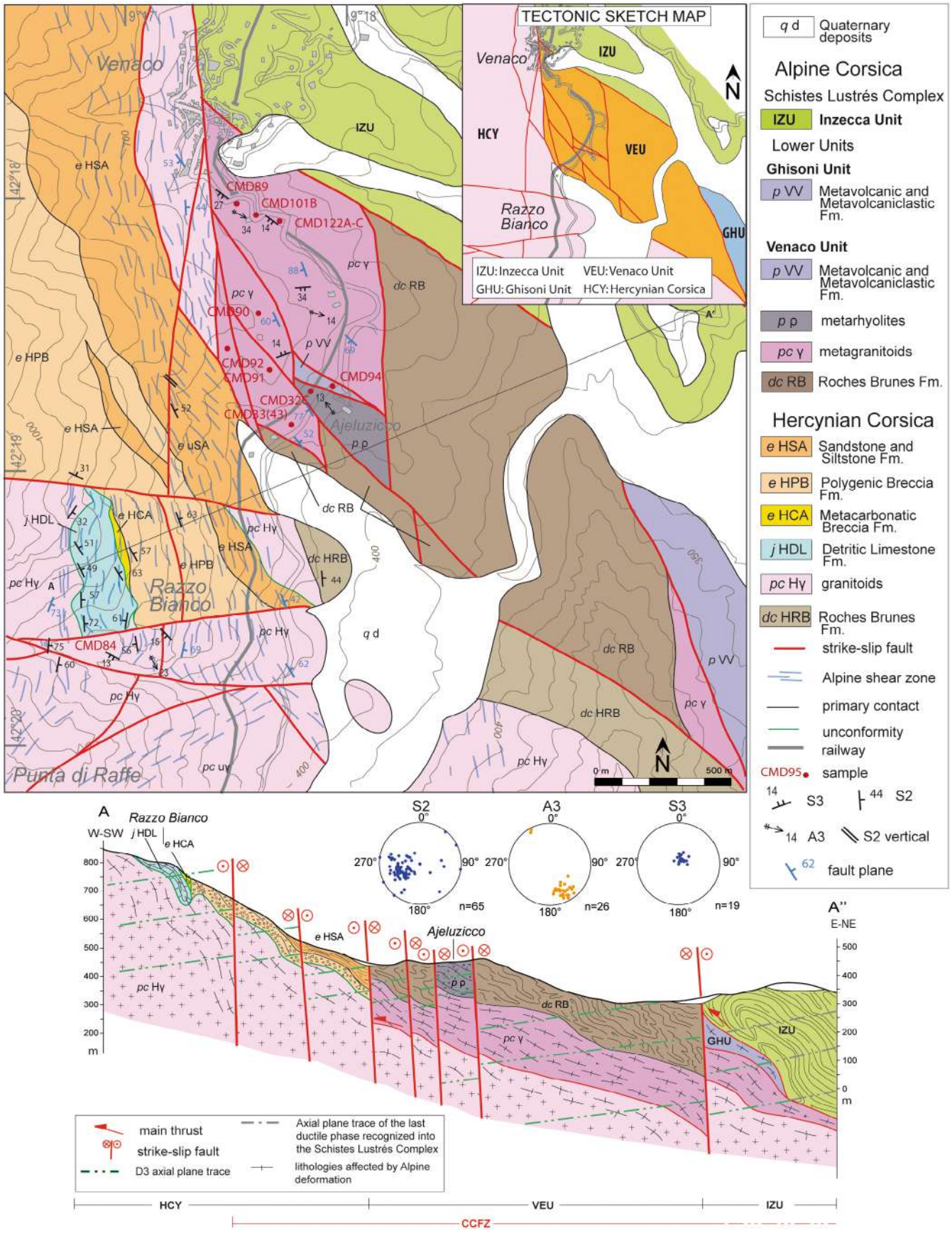

FIGURE 2 Legend on next page.

using the decay constants given by Steiger and Jäger (1977). Blanks were monitored after every three sample analyses. All parameters and relative abundance values are provided in supplementary data set and have been corrected for blanks, mass discrimination, and radioactive decay. Atmospheric ^{40}Ar was estimated using a value of the initial $^{40}Ar/^{36}Ar$ of 298.56 (Lee et al., 2006) Our criteria for the determination of a plateau are as follows: a plateau must include at least 70% of ^{39}Ar released, over a minimum of three consecutive steps agreeing at 95% confidence level. Plateau ages are given at the 2σ error level, and the plateau age uncertainties include analytical and J-value errors. All the errors on the inverse isochron, total fusion ages, and initial $^{40}Ar/^{36}Ar$ ratios are quoted at the 2σ error.

4 | RESULTS

The presence of a continental tectonic unit (i.e., Ghisoni Unit) belonging to the Lower Units in the study area (Figures 1 and 2) was recognized for the first time by Di Rosa and co-authors (Di Rosa, Frassi, et al., 2019; Di Rosa, Frassi, Malasoma, et al., 2020; Di Rosa, Frassi, Marroni, et al., 2020). These authors interpreted the portion of continental lithosphere cropping out between Venaco village and the Fium'Orbo valley as the northern portion of the Ghisoni Unit. In the light of the lithostratigraphic, structural and metamorphic evidence collected in this work, however, this portion of the Ghisoni Unit is here re-interpreted as an independent tectonic unit, named Venaco

TABLE 1 Representative EPMA analysis.

	Metapelites (sample CMD94)				Metagranitoids (sample CMD122)			
	S1 foliation		S2 foliation		S2 foliation			
Chl analyse	*Chl9*	*Phg31*	*Chl7*	*Phg30*	*Chl10*	*Chl3*	*Phg233*	*Phg238*
Wt%								
SiO_2	29.33	53.03	28.95	48.65	28.85	28.5	52.06	52.62
TiO_2	0.08	–	–	–	0.01	–	0.04	0.05
Al_2O_3	19.80	25.58	20.28	29.86	19.98	19.8	26.84	28.14
FeO	20.44	2.91	20.72	1.63	20.90	20.87	4.38	3.82
MnO	0.32	0.026	0.32	–	0.27	0.36	0.05	0.07
MgO	18.59	3.51	18.6	1.84	18.00	18.06	3.59	3.21
CaO	0.29	0.07	0.13	0.02	0.31	0.21	0.02	0.06
Na_2O	0.01	0.01	0.02	0.08	0.04	0.04	0.07	0.14
K_2O	0.08	9.95	0.02	10.53	0.03	0.02	9.84	10.13
tot.	88.93	95.09	89.04	92.61	88.40	87.87	96.89	98.23
Cations								
Si	2.95	3.53	2.91	3.32	3.14	2.91	3.43	3.41
Al^{IV}	1.05	0.47	1.09	0.68	1.15	1.09	0.57	0.59
Al^{VI}	1.30	1.53	1.31	1.73	1.41	1.30	1.51	1.56
Ti	0.01	–	–	–	–	–	–	–
Fe^{tot}	1.72	0.16	1.74	0.09	1.90	1.78	0.24	0.21
Mn	0.03	–	0.03	–	0.03	0.03	–	–
Mg	2.79	0.35	2.79	0.19	2.92	2.75	0.35	0.31
Ca	0.03	0.01	0.01	–	0.04	0.02	–	–
Na	–	–	–	0.01	0.01	0.01	0.01	0.02
K	0.01	0.84	–	0.92	0.01	–	0.83	0.88
Sum ox	14	11	14	11	14	14	11	11

FIGURE 2 Geological map, tectonic sketch, cross-section (A-A') and stereographic projections of Venaco Unit. In the sketch, HCY: Hercynian Corsica; VEU: Venaco Unit; GHU: Ghisoni Unit; IZU: Inzecca Unit (modified from Amaudric du Chaffaut et al., 1985). In the geological cross-section, figurative patterns were used in order to emphatize the differences in the rock types. The Roches Brunes Fm. is represented by discontinuous line that suggest the pre-Alpine deformation. For the Herynian granitoid, black crosses are used, which become stretched where the Alpine deformation occurs (they follow the orientation of the foliation). Detritic Limestone are represented by bricked pattern, whereas the breccias with small irregular empty dots. For metapelites (Permian Metacolvanic and Metavolcaniclastics and Eocene Sandstone and siltstone) a dashed line is used. The Inzecca Unit is represented by folded lines.

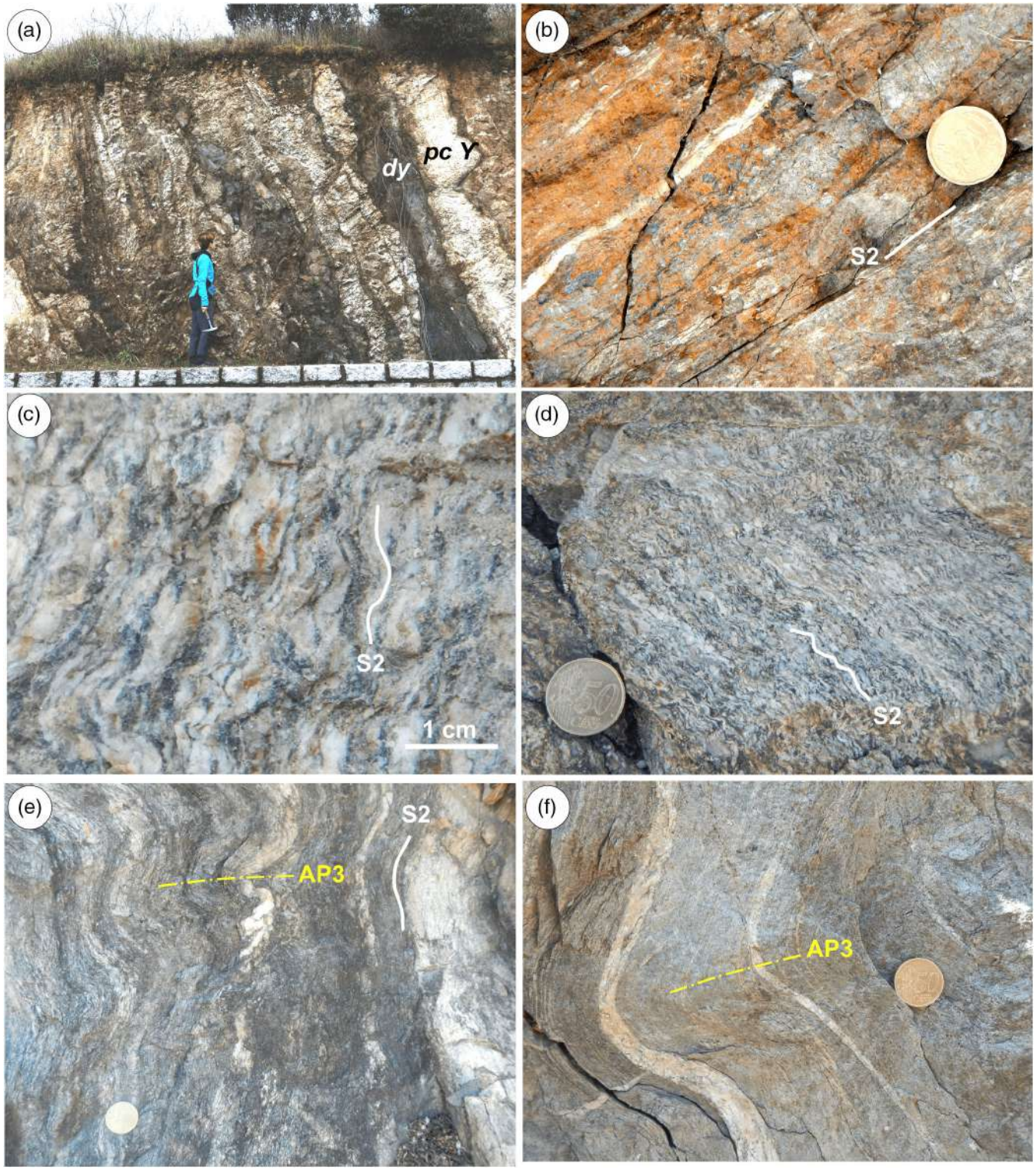

FIGURE 3 Mesoscopic structures and lithotypes of Venaco Unit. (a) Metagranitoids (*pc* γ) hosting mafic dyke (*dy*); (b) S2 foliation into the Roches Brunes Fm.; (c) folded S2 foliation in metagranitoids; (d) S2 foliation into metarhyolites; (e) S2 foliation, F3 fold and related axial plane foliation (AP3) into Metavolcanics and Metavolcaniclastic Fm. and (f) F3 fold and related axial plane foliation into the Metavolcanics and Metavolcaniclastic Fm.

Unit (VEU) (Figure 1). From the lithostratigraphic point of view, VEU differs from Ghisoni Unit because the metagabbros are lacking, whereas the metarhyolites are present (for a detailed description of Ghisoni Unit, see Di Rosa, Frassi, et al., 2019). Regarding the deformation style, the differences between VEU and Ghisoni Unit regard the degree of mylonitization reached during the D2 phase (see

Sections 4.1 and 4.2), which is combined with a different metamorphic condition (see Sections 4.3–4.5). Two strike-slip faults belonging to CCFZ separate VEU from the Hercynian Corsica, on the west, and the Schistes Lustrés Complex (i.e., Inzecca and Bagliacone-Riventosa Units), on the east (Figure 2). Its lower stratigraphic portion consists of Permian metagranitoids and is cut by mafic dykes (Figure 3a, Di Rosa, Farina, Lanari, & Marroni, 2020) intruded into a polymetamorphic rocks assemblage of Pan-African age (i.e., Roches Brunes Fm.; Figure 3b,c, Rossi et al., 1994). This basement is covered by a Permian meta-volcano sedimentary succession (i.e., Metavolcanic and Metavolcaniclastic Fm., e.g., Di Rosa, 2021), that consists of thin to medium layers of metapelites, metasandstones and fine-grained metabreccias interlayered with volcanic lavas mainly represented by metarhyodacites (Figures 2 and 3d–f).

4.1 | Mesostructures of VEU

VEU shows a polyphase deformation composed of three ductile events (D1-D3 phases), like those described for GHU by Di Rosa, Frassi, et al. (2019). In this work, unpublished data regarding the mesoscopic structural analyses are presented.

Relics of D1 phase (S1 foliation) was exclusively documented in the hinge zones of the F2 folds within fine-grained metasandstone and metapelites belonging to the Metavolcanic and Metavolcaniclastic Fm. The main structures documented in all the lithotypes can be assigned to D2 phase. In the metapelites, this phase produced F2 isoclinal folds with SSE–NNW trending A2 axis plunging less than 30° towards SE and an S2 axial plane foliation bearing a stretching L2 lineation trending ESE-WNW (Figure 2). The S2 foliation strikes NNW–SSE with variable dip due to the later D3 folding phase.

The metagranitoids show protomylonitic to ultramylonitic fabrics (Passchier & Trouw, 2005) with a S2 mylonitic foliation wrapping centimetre-sized quartz and feldspars grains showing strong shape preferred orientation and high aspect ratio (long axis/short axis: 13:3 and 9:3). The intrusive contact between metagranitoids and mafic dykes, even if locally deformed by F2 isoclinal folds, is mainly parallel to the S2 foliation documented in the metagranitoids (Figure 3a). A pervasive feature of the metagranitoids and Metavolcanics and Metavolcaniclastics Fm. is represented by syn-D2 quartz veins trending parallel to the S2 foliation (Figure 3e,f).

The last ductile phase (D3) was documented in the Metavolcanic and Metavolcaniclastic Fm. It produced open to close F3 asymmetric folds with sub-horizontal NW-SE trending A3 axes and S3 spaced axial plane foliation gently dipping to WSW (Figures 2 and 3e,f). The interference between F2 and F3 fold produced type 3 interference pattern (Ramsay, 1967). F3 folds affect the entire tectonic stack, constraining their coupling to have occurred before the D3 phase.

The last event documented in the field is responsible of the current architecture of the unit known as CCFZ (Figure 2, Bezert & Caby, 1989). It produced a N-S oriented, strike-slip system and related synthetic (ca. N170) and antithetical (ca. N90) faults, whose activity post-dates the exhumation of VEU and formed its present-day puzzling, similar to GHU described by Di Rosa, Frassi, et al. (2019) in the Fium'Orbo Valley.

4.2 | Microstructures of VEU

Metapelites were sampled in the Metavolcanic and Metavolcaniclastic Fm. cropping out along the road T20 south of Venaco (sample CMD94, Figure 2). In the metapelites, S1 foliation preserved in D2 microlithons, is a continuous, coarse-grained schistosity marked by the syn-kinematic growth of chlorite (Chl), phengite (Ph), quartz (Qtz) and albite (Ab) with minor K-feldspar (Kfs) and calcite (Cal) (Figures 3b and 4a). Chl and Ph related to the D1 phase reach 400 μm in length. The metamorphic minerals association grown during the D2 phase includes Chl, Phg and Qtz (Figure 4b). The syn-D2 phase Chl and Ph do not exceed 100 μm in length. Associated to the D2 phase, Qtz veins parallel to the S2 foliation are also found. At the microscale, the S3 foliation in metapelites is classifiable as a spaced crenulation cleavage associated with minor recrystallization of Cal and Qtz.

At the thin-section scale, the metagranitoids appear as pink biotite-bearing gneisses with monzogranitic compositions (i.e., suite U3 of Rossi et al., 2009) containing Qtz + Chl + Ab + sanidine (that replaces the former magmatic biotite) + Ms + Kfs + epidote (Ep) (Figure 4c–e). Accessory minerals are zircon, allanite, apatite and titanite. The original magmatic texture is almost completely overprinted by the D2 shearing deformation. The S2 foliation shows a mylonitic to ultramylonitic fabric marked by discontinuous layers of Ph + Chl ± biotite (Bt) and fine-grained recrystallized Qtz + KFs + Ab wrapping cm-grained Ab, plagioclase, and Qtz porphyroclasts (Figure 4c–e). The size of the white mica ranges between 50 and 200 μm. Kfs porphyroclasts into the metagranitoids of VEU (samples CMD92, CMD101b, CMD122A, locations are shown in Figure 2) has asymmetric tails (Figure 4a) and bookshelf structures associated to the main deformation phase (i.e., D2). Rare relics of magmatic Kfs wrapped by small crystals of phyllosilicates recrystallized during the D2 phase also occur. Qtz, found in both aggregates and in syn-D2 veins, is characterized by intracrystalline deformation such as undulatory extinction (Figure 4c), deformation bands and sub-grain rotation (Figure 4e). All related to the mylonitic S2 foliation. Qtz and Kfs textures corroborate the deformation temperatures of 300–400°C estimated for GHU by Di Rosa, Frassi, et al. (2019). The only structures related to the D3 phase are represented by microfolds affecting the phyllosilicate-rich layers.

The mafic dyke is composed of clinopyroxene (Cpx) + plagioclase (Pl) + amphibole (Amph) ± Qtz ± opaque oxides ± Ep (Figure 4f). The S2 mylonitic to ultramylonitic foliation is marked by an increase in intensity of foliation and a gradual decrease in size of Cpx and Pl porphyroclasts, which however preserve asymmetric tails indicating a top-to-W sense of shear (Figure 4f). Cpx are sometimes fractured and locally replaced by Chl and Pl (Di Rosa, Farina, Lanari, & Marroni, 2020). The intrusive magmatic contact between mafic dyke and metagranitoids is marked by the presence of large crystals (up to

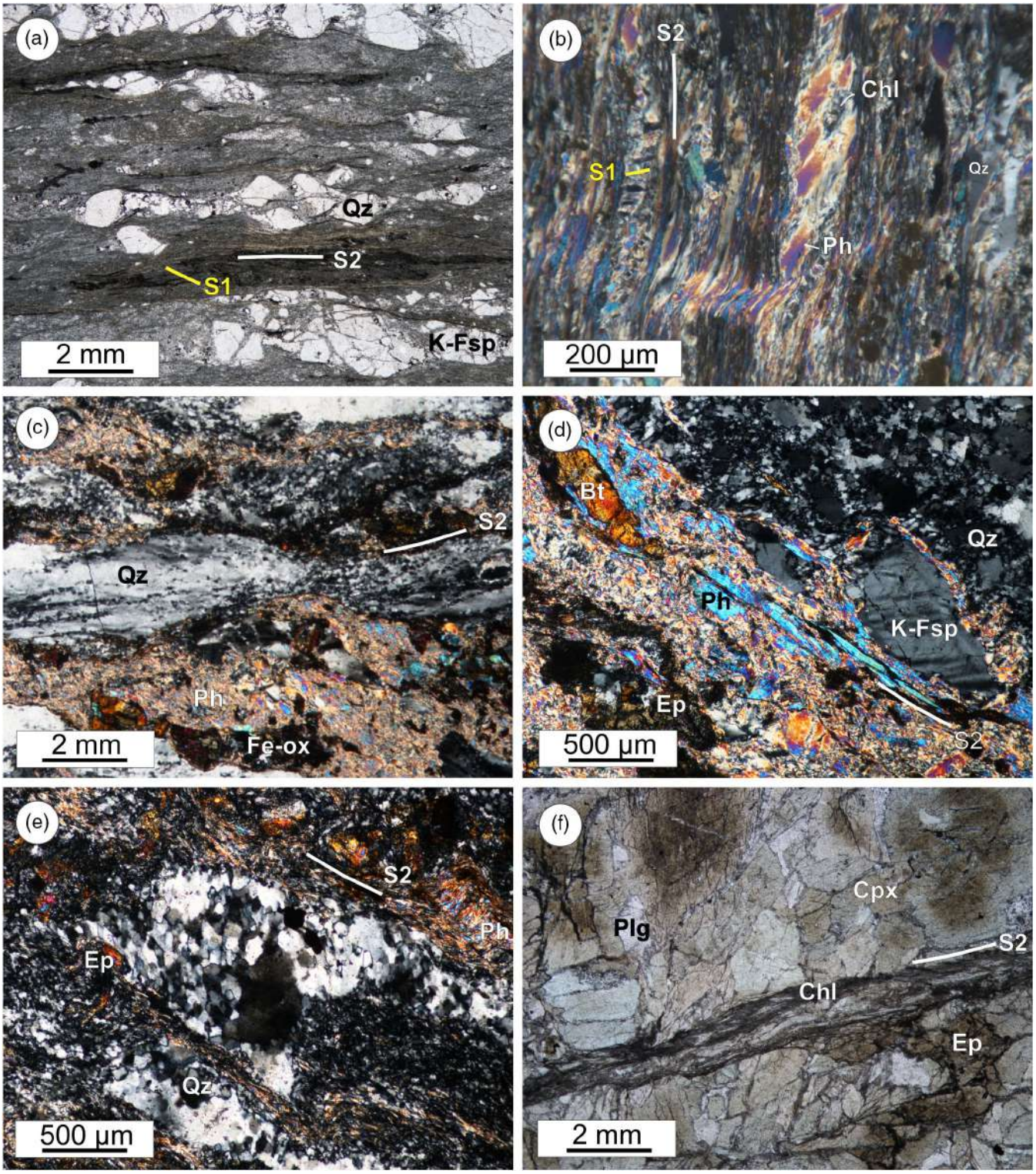

FIGURE 4 Microscopic structures of the Venaco Unit. (a) High strain cataclastic domain related to the S2 foliation in the Metavolcanics and Metavolcaniclastic Fm., sample CMD94 (plane-polarized light); (b) S1-S2 foliations in the Metavolcanics and Metavolcaniclastic Fm., sample CMD32C (cross-polarized light); (c) sub-grain rotation recrystallization mechanism in boudinaged quartz vein, marking the S2 foliation in metagranitoids. The necking of the vein and the S2 foliation are well shown, sample CMD92 (cross-polarized light); (d) white mica crystals grown along the S2 foliation into metagranitoids, sample CMD92 (cross-polarized light); (e) sub-grain rotation fabric in metagranitoids, sample CMD122A (cross-polarized light) and (f) µ-shear zone parallel to the S2 foliation into the mafic dyke, sample CMD122B (plane-polarized light). Qz: quartz; Chl: chlorite; Ph: phengite, Fe-ox: iron oxides; Bt: biotite; Ep:epidote; K-Fsp: K-feldspar; Cpx: clinopyroxene.

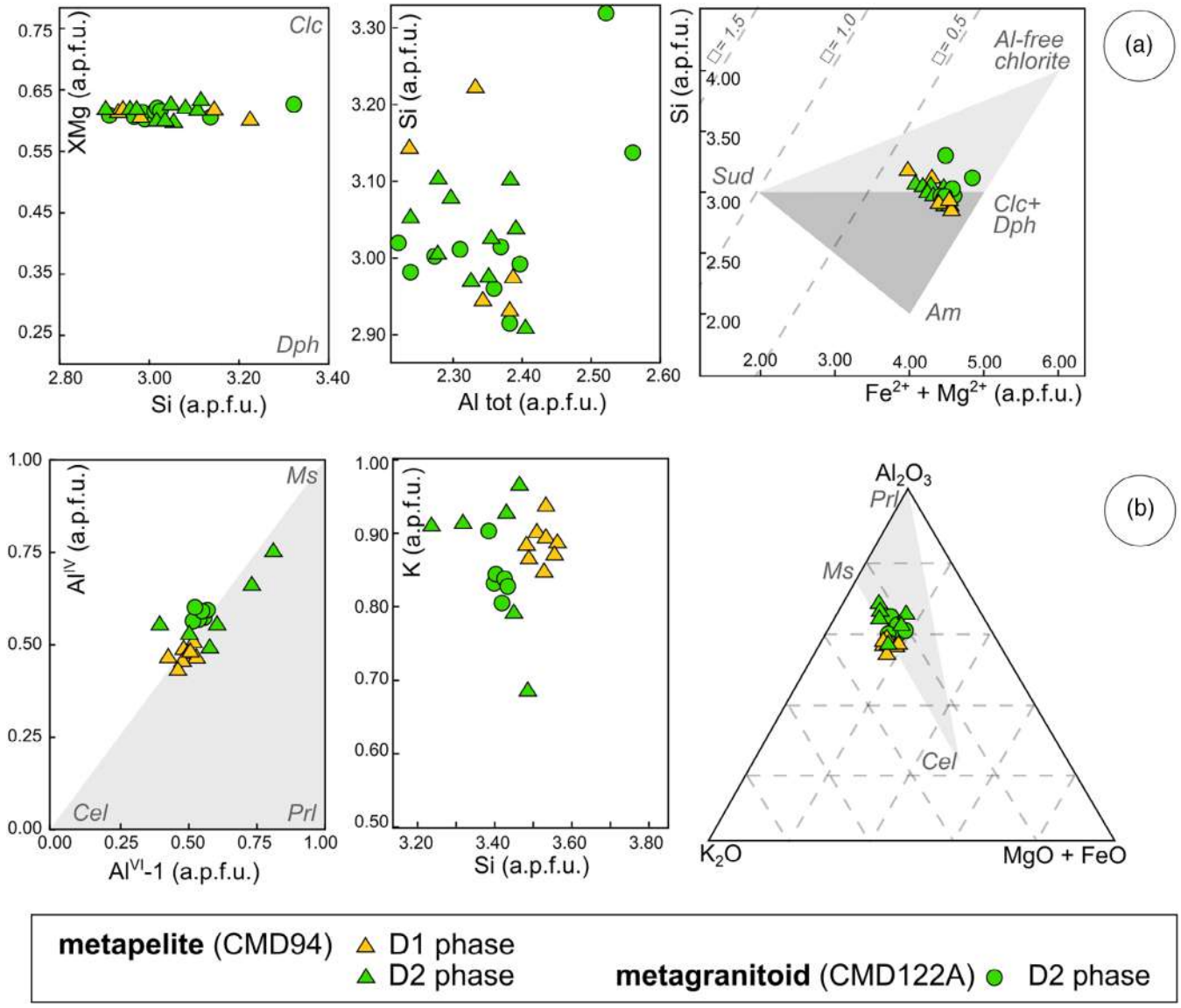

FIGURE 5 Mineral chemistry of (a) chlorite and (b) phengite found along the S1 and S2 foliations of the metapelite sample CMD94 and along the S2 foliation of the metagranitoid sample CMD122. In (a): dark and pale grey triangles indicate the compositional spaces delimited by chlorite end-members, defined by Vidal and Parra (2000) and Inoue et al. (2009), respectively. Am: amesite, Clc: clinochlore, Dph: daphnite, Sud: sudoite, empty square: vacancies (a.p.f.u.). In (b): grey triangles in the Al^{VI}-1 vs. Al^{IV} and the ternary diagrams indicate the phengite solid solutions from Bousquet et al. (2002) and from Vidal and Parra (2000), respectively. Cel: celadonite, Prl: pyrophyllite, Ms: muscovite.

250 μm) of Aln hosted by the metagranitoid, which appear fractured and filled by Ep and of apatite (Ap).

4.3 | Mineral chemistry of chlorite and phengite

Syn-kinematic Chl and Ph crystals were selected in the metapelite and metagranitoid within structural sites related to the D1 (i.e., the S1 foliation) and the D2 phases (i.e., the S2 foliation).

In metapelite (sample CMD94), chlorites grown along the S1 foliation are characterized by Si and Al contents ranging between 2.93–3.23 and 2.23–2.38 atom per formula unit (a.p.f.u., Table 1), respectively, and by an XMg slightly higher than 0.50, indicating a predominance of the clinochlore end-member (Figure 5a). Within the compositional space, which includes chlorite having Si content higher than 3 a.p.f.u. (e.g., Inoue et al., 2009), these low-Al chlorites fall nearby the solid solution between sudoite and Clc + daphnite end-members. Having Si content ≈3 a.p.f.u. and the total content of Mg + Fe^{2+} in the M1-M4 octahedral sites greater than 3.5 a.p.f.u., the vacancies of D1 phase Chl do not exceed 0.50 a.p.f.u. (see Figure 5a). A second Chl generation crystallized along the S2 foliation has been found (Figure 4b). Si content in the D2 Chl (2.83–3.10 a.p.f.u.) is on average lower than those of the D1 phase Chl (Figure 5a). D1 and D2 phase Chl have instead similar Al, Fe^{2+}+Mg^{2+} contents and XMg,

which determine also for this second generation an affinity for the Clc and-member and a vacancies content, which never exceed 0.5 a.p.f.u. (Figure 5a).

In metagranitoids (CMD122A), the analysed chlorites are related to the D2 phase. They show a more variable content in Si and Al than those of the metapelites (2.91–3.32 and 2.22–2.56 a.p.f.u.,

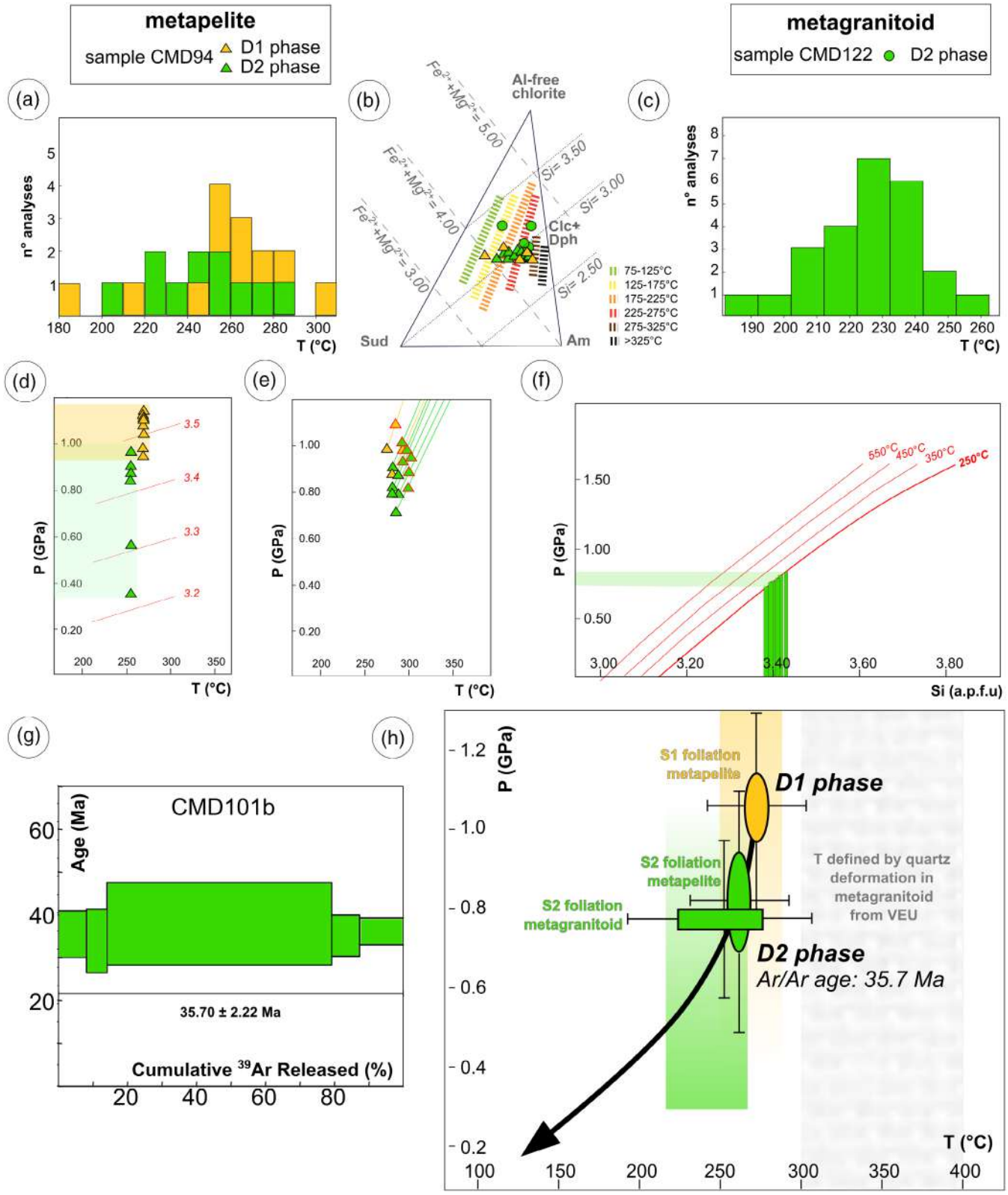

FIGURE 6 Legend on next page.

respectively): this determines a greater variability of the end-members proportion. However, also these Chl tend to be magnesian (Figure 5a).

Phg has been found along the S1 and S2 foliations in metapelite (CMD94) and along the S2 foliation in metagranitoid (CMD122). All the analysed Ph roughly plots along the perfect solid solution between celadonite and Ms end-members, with those belonging to the D1 phase of the metapelite markedly tending towards the Al-poor end-member (Table 1 and Figure 5b). D1 phase phengites are characterized by a very homogeneous composition, with moderately high Si content (≈ 3.50 a.p.f.u.) and K content between 0.85 and 0.95 a.p.f.u. (Figure 5b). D2 phengites from metapelite have heterogeneous composition determining a wide range of end-member proportions, which however tends to the Ms end-member (Figure 5b). The D2 phase phengites of the metagranitoid have Si (3.39–3.43 a.p.f.u.), K (0.81–0.09 a.p.f.u.) and Al (2.08–2.18 a.p.f.u.) contents comparable with those of the D2 Phg from metapelites (Figure 5b).

4.4 | Thermobarometry on metapelite

Temperature and pressure estimates of the metapelite and metagranitoid were obtained using different methods (Figure 6a–f). *T* in metapelites were calculated using the composition of Chl crystallized along the S1 and S2 foliations (CMD94). The calibrations of Cathelineau (1988) as well as those of Bourdelle and Cathelineau (2015) which includes the chlorites having Si content >3 a.p.f.u., depict a wide thermal range where the chlorite of the D1 phase is in equilibrium (180–310°C, Figure 6a,b respectively) within which, however, a peak between 250 and 280°C is clearly identified. Lower *T* (<225°C) are related to chlorites having Si >3 a.p.f.u. (Figure 6b). Similarly, chlorites sampled along the S2 foliation seem to balance out at different temperatures (200–290°C), but with a maximum in the 220–260°C range (Figure 6a,b).

Pressure equilibrium conditions during the D1 and the D2 phases were calculated by using Si in Ph calibration (Bousquet et al., 2002; Figure 6d) and with the Ph-Qtz-water method (Dubacq et al., 2010; Figure 6e,g). In both cases, the calculations were obtained by fixing the *T* value to 260°C (D1 phase) and 250°C (D2 phase) resulting from the temperature previously estimated, choosing the most representative value obtained by the different thermometers applied (see above). Si in Phg allowed to constrain the *P* ranges of the D1 phase to 0.90–1.10 GPa and of the D2 phase to 0.35–0.95 GPa (Figure 6d). A less dispersed result is obtained with the Dubacq's calibration (Dubacq et al., 2010; Figure 6e) which was obtained fixing the water activity to 0.9, compatible with the calcite content of the metapelite (for details see also Frassi et al., 2022) and admitting only the *P* conditions for which the optimal water content (in this case 93%–95%) is the same for the greatest amount of analysis. By comparing the results, we can identify two peaks that are 0.90–1.10 GPa for the D1 phase and 0.70–1.00 GPa for the D2 phase. We were not able to obtain satisfactory *P*–*T* estimates with the Chl-Ph-Qtz-water method of Vidal and Parra (2000), since no Chl-Ph couple was able to equilibrate with energy conditions below 1000 J.

4.5 | Thermobarometry on metagranitoids

Temperature conditions related to the D2 phase of the metagranitoid (sample CMD122A) were calculated using two calibrations. Applying the calibration of Bourdelle and Cathelineau (2015), Figure 6b), our data are included in the *T* range of 125–325°C. Less dispersed are the results obtained by applying the Cathelineau and Nieva (1985) thermometer (180–260°C), based on the Al^{IV} content of Chl (Figure 6c). However, with both the calibrations a peak between 225 and 275°C could is identified.

Microstructures in Qtz and feldspar described in Section 4.2, indicate that dislocation creep represents the main deformation mechanism in Qtz during the development of the main foliation, suggesting deformation *T* of 300–400°C (Stipp et al., 2002). Microstructures in feldspar suggest deformation *T* of 400–450°C (Passchier & Trouw, 2005).

Pressure conditions of the D2 phase of the metagranitoid were obtained applying the Massonne and Schreyer (1987) calibration based on the Si content in Ph, assuming a fixed *T* value of 250°C. Most of the phengite analysis yield *P* values of 0.75–0.80 GPa (Figure 6f).

4.6 | $^{40}Ar/^{39}Ar$ dating

As documented in Section 4.3, the most pervasive structure documented in the metagranitoids is the S2 foliation. No evidence of D1 domains or Chl/Ph composition comparable to those grown along the S1 in metapelites were documented in metagranitoids samples. As a consequence, metagranitoids represent the ideal lithotype to

FIGURE 6 Thermobarometric results from metapelite and metagranitoid. (a) Chlorite-based thermometer, calibration of Cathelineau (1988); (b) chlorite-based thermometer, calibration of Bourdelle and Cathelineau (2015); (c) chlorite-based thermometer, calibration of Cathelineau and Nieva (1985); (d) phengite-based geobarometer, calibration of Bousquet et al. (2002). Red lines indicating Si content in phengite (a.p.f.u.); (e) Dubacq et al. (2010) calibration based on the water content in phengite. Calculations were performed fixing water activity to 0.9, % of Fe^{3+} to 0.32 of Fe_{tot} and the T to 260 and 250°C for the D1 and D2 phases, respectively. Data rimmed in black and red indicate 95% or 93% of water, respectively. The reactions that define the equilibrium are (1) pyrophyllite = pyrophylliteH + water, (2) 3 Mg-celadonite + 4 pyrophyllite = 11 alpha-quartz + 2 muscovite + phlogopite + 2 pyrophylliteH, (3) 3 Mg-celadonite + 2 pyrophyllite = 11 alpha-quartz + 2 muscovite + phlogopite + 2 water and (4) 3 Mg-celadonite + 2 pyrophylliteH = 11 alpha-quartz + 2 muscovite + phlogopite + 4 water; (f) phengite-based geobarometer, calibration of Massonne and Schreyer (1987); (g) $^{40}Ar/^{39}Ar$ age spectra as a function of ^{39}Ar released. The error boxes of each step are at the 2S level. The error of ages is given at the 2S level. Ages were calculated using the ArArCalc software (Koppers, 2002) Raw data are presented in Data Set S1; (h) synthesis of the P–T–t conditions obtained from metapelite and metagranitoid of VEU in the area south of Venaco (D1 and D2 VEU).

constrain the age of S2 foliation. For this reason, a metagranitoid sample (CMD101b) poorly weathered and collected far from both D2 shear zones and cataclastic zones related to the activity of the CCFZ, were selected to obtain metamorphic white mica recrystallized during the D2 phase, used for single grain ^{40}Ar-^{39}Ar step-heating analysis. A single white mica grain yielded a plateau age of 35.7 ± 2.22 Ma, which corresponds to 100% of ^{39}Ar released and to five steps. The inverse isochron for the plateau steps provides a concordant age at 35.25 ± 3.89 Ma. It is important to underline that the $^{40}Ar/^{39}Ar$ dating of VEU was performed on the phengite crystallized on the S2 foliation of the metagranitoids.

An age of 35.7 ± 2.22 Ma can be considered as the most accurate age (Figure 6g and Appendix S1).

5 | DISCUSSION

5.1 | *P–T-d-t* path of VEU

Linking the *P* and *T* conditions obtained using the chlorites and phengites grown along the S1 and S2 foliation a *P–T-d* path of VEU can be constructed (Figures 6h and 7). The *P–T* conditions of 0.9–1.10 GPa and 260°C for the D1 phase have been calculated from metapelites (sample CMD94) using the Chl and Ph recrystallized along the S1 foliation. Due to the lack of evidence for an older relic foliation, the D1 phase can be regarded as the deformation event during which VEU reaches its maximum depths. Considering that the lithostatic pressure exerted on the Lower Units is given by metamorphic rocks of both oceanic and continental affinities, we assume an average crustal geobaric gradient of 30 MPa/km (Best, 2003). Therefore, basing on the pressure registered by VEU during the D1 phase, peak conditions occurred at the depth of ≈ 33 km (Figure 6h). We have also identified a second *P–T* event recorded by the chlorites and phengites crystallized along S2 foliation in metapelites which constrain the *P* and *T* conditions of the D2 phase at 0.70–1.00 GPa and 250°C. These data are coherent with the *P–T* estimates for the D2 phase obtained in metagranitoids (i.e., 0.75–0.80 GPa and 225–275°C). Overall, all the collected data indicate that the D2 phase developed during a retrograde path at depth of ≈ 26 km (Figure 6h).

Temperatures obtained for the D2 phase using microstructure- and petrology-based thermometers in metagranitoids is apparently in contrast. The activity of chlorite end-members as well as Al^{IV} in Chl thermometers applied to the chlorite analysis of the metagranitoid (sample CMD122) indicate a temperature of max. 275°C, whereas microstructures of Qtz and feldspar indicate deformation temperatures of about 400°C (Figure 6c,f,h). This discrepancy, already described by Di Rosa, Frassi, Malasoma, et al. (2020) for GHU in the Fium'Orbo valley, could be reduced including the error of 20°C associated to the quantitative methods used to determine the *T* (e.g., Bourdelle & Cathelineau, 2015). The presence of syn-D2 veins into the metagranitoids suggests that the process of hydrolytic weakening was activated producing the overestimation of the deformation temperature (Law, 2014). We can so propose a reliable *T* range for the D2 phase registered by VEU between 270 and 280°C.

The geothermal gradient of 7°C/km calculated for VEU using the recommendation of Best (2003) is comparable to those obtained from *P–T-d* paths of other Lower Units (Di Rosa, De Giorgi, Marroni, & Vidal, 2017; Di Rosa, Frassi, et al., 2019; Di Rosa, Frassi, Malasoma, et al., 2020; Di Rosa, Meneghini, et al., 2019; Frassi et al., 2022). The *P–T-d* path obtained for the VEU however indicates that the exhumation of the unit occurred under isothermal conditions (Figure 7). The 'shape' of its retrograde path is however similar to the retrograde path of Castiglione-Popolasca and Ghisoni units (i.e., Lower Units located immediately above the Hercynian Corsica, Di Rosa, Frassi, et al., 2019). For these units, the retrograde isothermal path can be explained assuming a fast exhumation stage during which the temperature peak does not exceed the temperature achieved at pressure peak (e.g., Di Rosa, Frassi, et al., 2019), up to shallow structural levels. Conversely, most of the Lower Units show a warmed path (i.e., Croce d'Arbitro, Piedigriggio-Prato, Canavaggia, Pedani, Scoltola and Tour de Valletto units) during which the exhumation of continental units occurred together with a substantial (>100°C) increase of temperature (e.g., Frassi et al., 2022).

Moreover, it is important to underline that the $^{40}Ar/^{39}Ar$ dating of VEU was performed on the phengite crystallized on the S2 foliation of the metagranitoids. Considering the temperature estimates in this work from D2 syn-kinematic chlorites and phengites of VEU at a maximum of 280°C we interpret the isotopic age at ± 2.22 Ma obtained for syn-kinematic phengite as the crystallation age.

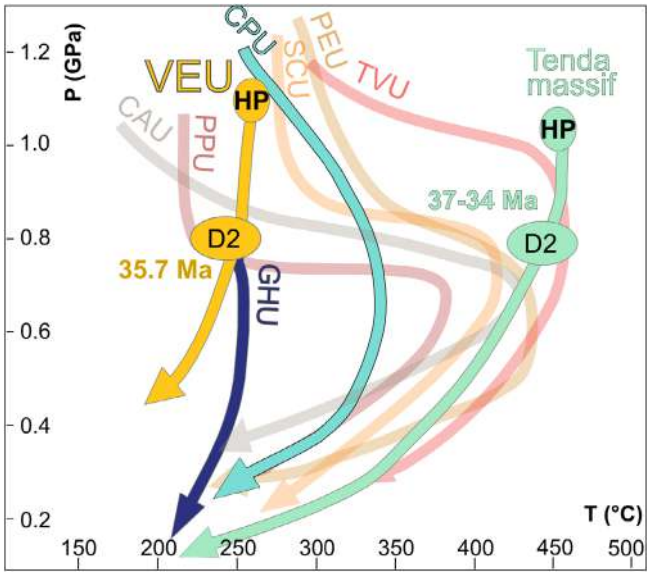

FIGURE 7 The *P–T-d* conditions of European continental units. VEU: Venaco Unit, this work. From the Fium'Orbo area: Ghisoni Unit (GHU, from Di Rosa, Frassi, et al., 2019). From Corte area: Castiglione-Popolasca (CPU), Piedigriggio-Prato (PPU) and Tour de Valletto (TVU) Units (Di Rosa, Frassi, et al., 2019; Frassi et al., 2022). From Cima Pedani area: Canavaggia (CAU), Scoltola (SCU) and Pedani (PEU) Units (Di Rosa, Meneghini, et al., 2019). Tenda Massif path is taken from Molli et al. (2006).

No thermobarometric estimates are available for the D3 phase because of the lack of phyllosilicates crystallizations along the S3 foliation. According to the map-scale structures (Di Rosa, De Giorgi, Marroni, & Pandolfi, 2017; Malasoma et al., 2020), this phase occurred when the units were already stacked and contributes to the final exhumation of the Alpine Corsica, corroborating what had been already suggested for the late stage of exhumation of the Lower Units (Daniel et al., 1996; Di Rosa, Frassi, Marroni, et al., 2020; Fournier et al., 1991; Jolivet et al., 1991; Zarki-Jakni et al., 2004). The ages obtained by apatite fission tracks, which range from 35 to 25 Ma in southern Hercynian Corsica, to <25 Ma, in central Hercynian Corsica (Danišik et al., 2007), testify this later extensional tectonics, probably driven by the progressive collapse of Alpine Corsica associated with rifting in the Ligurian-Provençal back-arc basin.

5.2 | Metamorphism and age constraint: Implications for Alpine Corsica evolution

In the Alpine Corsica, the remnants of the European continental margin deformed and metamorphosed under *HP* metamorphic conditions have been identified in the Tenda Massif, located in northeastern Corsica within the Alpine Domain (Gibbons & Horak, 1984; Maggi et al., 2012; Molli & Tribuzio, 2004; Tribuzio & Giacomini, 2002) and in the Lower Units cropping out with a north–south trend along the boundary between Hercynian and Alpine Corsica (Bezert & Caby, 1988; Di Rosa, De Giorgi, Marroni, & Pandolfi, 2017; Di Rosa, Frassi, et al., 2019; Garfagnoli et al., 2009; Malasoma et al., 2006). In addition, evidence of Alpine deformation has been found also in the eastern rim of the Hercynian Corsica, along localized shear zones close to the boundary with the Alpine Corsica (Amaudric du Chaffaut & Saliot, 1979; Di Rosa, Frassi, Marroni, et al., 2020; Di Vincenzo et al., 2016; Frassi et al., 2022; Rossi et al., 1994).

Most of the geodynamic reconstructions (Beaudoin et al., 2017; Di Rosa, Meneghini, Marroni, et al., 2020; Malavieille et al., 1998; Marroni et al., 2017; Molli, 2008) indicate that the European continental margin was dragged downward in an east-dipping subduction zone during the Early Tertiary. It is during this stage that they acquired the *HP* metamorphic imprint.

Age constraints of this *HP* metamorphism were obtained from the East Tenda shear zone (Figure 1), a crustal-scale ductile shear zone with a complex kinematics originated during the underthrusting of the Tenda Massif in the subduction zone (Molli et al., 2006) and reactivated in extensional regime during exhumation (e.g., Jolivet et al., 1990). The age of the underthrusting event is roughly constrained to Early Eocene (Ypresian) by Brunet et al. (2000) that indicate a maximum age of 46.6 ± 1.2 Ma by phengite $^{40}Ar/^{39}Ar$ geochronology and by Maggi et al. (2012) that provide for the same event a U–Pb rutile age of 54 ± 8 Ma. The available data indicate that the Tenda Massif was buried at a depth between 30 and 40 km (Figure 8a; Gibbons & Horak, 1984; Maggi et al., 2012; Molli et al., 2006; Molli & Tribuzio, 2004; Rossetti et al., 2015). The ages of 34–37 Ma (Priabonian), reported by Vitale Brovarone and Herwartz (2013) and by Brunet et al. (2000) for the East Tenda shear zone, constrain the exhumation of the Tenda Massif at 25–30 km of depth (Molli et al., 2006). This picture is recently confirmed by Beaudoin

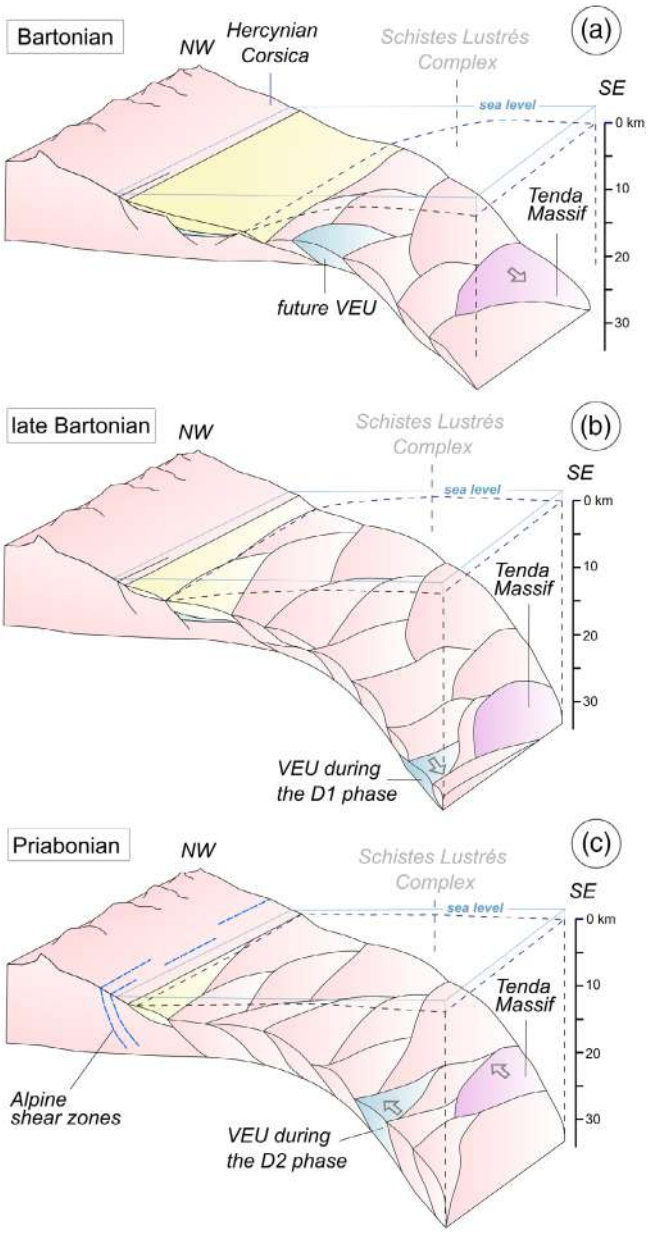

FIGURE 8 3D tectonic sketch model showing the subduction of the European continental margin and the consequent exhumation of the resulting tectonic units in a still compressive setting. (a) The stage of subduction in the Bartonian: Tenda Massif is parked at ≈ 25–30 km of depth, VEU is next to the subduction and the foredeep deposits are settling on the margin; (b) during the late Bartonian, VEU is supposed to be at the maximum depth of ≈ 33 km and is deforming by the D1 phase while the Tenda Massif stands and heats up at ≈ 25–30 km; (c) in the Priabonian, VEU is quickly exhumed (D2 phase) and reach the Tenda Massif at about 26 km. Pink is used for both the Hercynian Corsica and the subducted Lower Units in order to underline their provenance. VEU and the Tenda Massif are differentiated from the other Lower Units (blue and violet, respectively). Arrows indicate the kinematics of the Lower Units during their subduction and exhumation. Modified from Di Rosa (2021) and reference therein.

et al. (2020), that constrain the end of burial and exhumation at ~34 and ~22 Ma (Priabonian and Aquitanian), respectively.

The other *HP* continental units (i.e., Lower Units) are characterized by a metamorphic sequence whose youngest deposits are represented by foredeep turbidites showing Bartonian microfossils in the uppermost stratigraphic levels (Bezert & Caby, 1988). This finding indicates that the underthrusting event and the related *HP* metamorphism probably occurred during the late Bartonian (i.e., after 41.2 Ma, Figure 8b). This evidence is coherent with the age of 35.7 Ma (Priabonian) that we obtained for the D2 event (i.e., the retrograde path) in the metagranitoids of VEU. A recent ^{40}Ar-^{39}Ar age of 38.0 ± 0.2 Ma obtained for the Lower Units in the Golo Valley (i.e., Croce d'Arbitro Unit by Rossetti et al., 2022) support our ^{40}Ar-^{39}Ar datings for VEU.

Alpine metamorphism was also found within top-to-the west shear zones occurring in the easternmost sector of the Hercynian Corsica (Di Rosa, De Giorgi, Marroni, & Pandolfi, 2017; Malasoma et al., 2020; Rossi et al., 1994). The dating of these shear zones indicates for the Alpine metamorphism a minimum age of ≈ 46 Ma by (^{40}Ar/^{39}Ar white micas; Di Vincenzo et al., 2016). As discussed by Di Rosa, Frassi, Marroni, et al. (2020) these ages are in contrast with the Lutetian-Bartonian age of metabreccias and metasandstones affected by shear deformation. On the contrary, the Priabonian ages (≈ 37 and 35 Ma, Figure 8c) that we obtained for VEU perfectly fit.

Re-equilibration during exhumation at ≤33–32 Ma (Rupelian) is also suggested by Di Vincenzo et al. (2016) and interpreted by Di Rosa, Frassi, Marroni, et al. (2020) as developed during the exhumation of the eastern rim of the Hercynian Corsica.

The age constraint available for the Tenda Massif and Lower Units can be framed into a coherent picture where the age of HP metamorphism achieved by the continental crust fragments during the underthrusting is progressively younger moving from northeast to southwest: Ypresian in the Tenda Massif, Bartonian in the Lower Units and probably Priabonian or younger in the westernmost rim of the Hercynian Corsica (VEU). These data indicate that even if the Lower Units and the Tenda Massif were subducted at different times but at 34–36 Ma (Priabonian), they were at the same exhumation depth, whereas the westernmost rim of Hercynian Corsica was deformed by the top-to-W shear zones (Di Rosa, Frassi, Marroni, et al., 2020).

5.3 | Geodynamic implications

To reconstruct the progressive involvement of the thinned European continental margin in the E-dipping subduction zone, we compare the age of metamorphism here presented for the VEU (i.e., Lower Units) with those available for the continental unit of the Tenda Massif and Croce d'Arbitro (the only continental unit of Alpine Corsica with isotopic age constraints; Brunet et al., 2000; Maggi et al., 2012; Rossetti et al., 2022). The involvement of the continental crust in the subduction zone followed the underthrusting of the last portion of the Ligure-Piemontese oceanic crust. The data available for the Internal Ligurian Units (i.e., the best-preserved fragments of the Ligure-Piemontese basins exposed along the Alpine Corsica – Northern Apennines transect) indicate that in the early Palaeocene, some portions of oceanic crust were not yet involved in the subduction zone (Marroni, 1991; Marroni et al., 2017; Meneghini et al., 2020; Molli, 2008). The first sector of continental crust involved in the subduction zone was probably the sector currently represented by the Tenda Massif (i.e., the continental fragment showing the oldest *HP* metamorphic imprint). The involvement of the continental crust continued with the underthrusting of the more internal areas of the European margin, today represented by the Lower Units. Subsequently, also the westernmost rim of the Hercynian Corsica is involved in the same subduction zone.

The data available and those provided in this paper suggest that the Tenda Massif and the VEU (Lower Units) were dragged downward at different times (i.e., Ypresian for the Tenda Massif and Bartonian for the VEU), but both were exhumed simultaneously during the Priabonian. Consequently, these two units experienced different stationary time at depth, controlled by several boundary conditions as suggested by Frassi et al. (2022), like exhumation rate, exhumation trajectory, thermal state of the overriding plate and mechanical and rheological characteristics of the downgoing continental crust. The occurrence of European continental units characterized by different stationing time at depth has been described for the first time by Di Rosa, Frassi, et al. (2019). According to these authors, the different stationing time at depth is correlated to the structural position within the subduction channel: the units with isothermal paths are located at the base of the subduction channel immediately over the Hercynian Corsica, whereas the units with warmed paths are located at its top, below the Schistes Lustrés Complex. Following this distinction, the *P–T* data related to the Tenda Massif, that experienced a warmed path (Molli & Tribuzio, 2004), indicate that this continental slice experienced a long stationary time at depth before its exhumation. On the contrary, the data provided in this paper for the VEU indicate an isothermal path and then an exhumation predated by a short stationary time at depth.

6 | CONCLUSIONS

In this paper, the *P–T-d* path of the VEU is reconstructed and combined to the ^{40}Ar/^{39}Ar dating of syn-kinematic muscovite to present the first *P–T-d-t* path of a Lower Units. The proposed scenario indicates that the VEU reached the baric peak (D1 phase) at ≈ 33 km of depth in the Bartonian time (post 41.2 Ma). At 35.7 Ma (middle Priabonian), VEU was exhumed at shallower structural level (≈ 26 km of depth) mainly through the activation the D2 top-to-W shear zones. The retrograde isothermal path of the VEU indicates that its stationary time at depth of ca. 33 km (D1 phase) was minimum and that after reaching the maximum depth it is "quickly" exhumed. During this fast rise, VEU completed its deformation history throught the D2 phase, registered at ca. 26 km, and the D3 phase at shallower depths.

The comparison of the new isotopic data presented in this contribution with the only one available for a continental unit (i.e., Tenda Massif) allows proposing a new scenario for the progressive involvement of the thinned European continental margin in the east-dipping subduction zone. This scenario includes the underthrusting of the continental fragments in different time and in different structural positions within the subduction channel of the alpine orogenic wedge. Each fragment underwent thus a different stationing time at depth, as indicated by the "shape" of the *P–T-d* path, and then started to be exhumed together within the subduction channel. This behaviour can be proposed as effective for all the *HP* continental units during the continental subduction and must be thus considered to understand the geological processes related to the collisional orogens.

AUTHOR CONTRIBUTIONS

Maria Di Rosa collected data during fieldwork and prepared the geological map of the study area and performed the thermobarometry. E. Sanità, M. Corsini and J. M. Lardeaux contributed with the Ar-Ar analysis, Maria Di Rosa, M. Marroni and L. Pandolfi interpreted the data and developed the conceptual model. Maria Di Rosa, M. Marroni and C. Frassi prepared the manuscript with contributions from all co-authors.

ACKNOWLEDGEMENTS

This work was supported by Prin 2020 resp. Michele Marroni. We thank Andrea Risplendente for microprobe analysis. We also thank the editor Ian Somerville, André Michard and an anonymous reviewer for the constructive notes.

CONFLICT OF INTEREST STATEMENT

The author declares no conflict of interest.

DATA AVAILABILITY STATEMENT

The data that support the findings of this study are available from the corresponding author upon reasonable request.

ORCID

Maria Di Rosa https://orcid.org/0000-0002-1154-7429
C. Frassi https://orcid.org/0000-0002-7522-9905

REFERENCES

Agard, P. (2021). Subduction of oceanic lithosphere in the Alps: Selective and archetypal from (slow-spreading) oceans. *Earth-Sciences Reviews*, *214*, 103517.

Alessandri, J. A., Magné, J., Pilot, M. D., & Samuel, E. (1977). Le Miocène de la région de Corte-Francardo. *Bulletin de la Société Scientifique de Histoire Naturelle de la Corse*, *622*, 51–54.

Amaudric du Chaffaut, S., Bonin, B., Caron, J. M., Conchon, O., Rossi, P., Bimbier, A., Damiani, L., Dominici, R., Heetveld, H., & Rouire, J. (1985). Carte Géologique de la France, feuille Venaco (1114). BRGM, scale 1: 50000, 1 sheet.

Amaudric du Chaffaut, S., & Saliot, P. (1979). La region de Corte: sectèur-clè pour la comprehension du métamorphisme alpine en Corse. *Bulletin de la Société Géologique de France*, *21*, 149–154.

Beaudoin, A., Augier, R., Jolivet, L., Jourdon, A., Raimbourg, H., Scaillet, S., & Cardello, G. L. (2017). Deformation behavior of continental crust during subduction and exhumation: Strain distribution over the Tenda massif (alpine Corsica, France). *Tectonophysics*, *705*, 12–32. https://doi.org/10.1016/j.tecto.2017.03.023

Beaudoin, A., Scaillet, S., Mora, N., Jolivet, L., & Augier, R. (2020). In Situ and step-heating 40Ar/39Ar Dating of white mica in Low-temperature shear zones (Tenda Massif, Alpine Corsica). *Tectonics*. https://doi.org/10.1029/2020TC006246

Best, M. G. (2003). *Igneous and metamorphic petrology* (2nd ed.). Blackwell.

Bezert, P., & Caby, R. (1988). Sur l'age post-bartonien des événements tectonométamorphiques alpins en bordure orientale de la Corse cristalline (Nord de Corte). *Bulletin de la Société Géologique de France*, *4*(6), 965–971.

Bezert, P., & Caby, R. (1989). La deformation progressive de l'Eocene de la re´gion de Corte: nouvelles donne´es petrostructurales et conse quences pour la tectogenese Alpine en Corse. *Comptes-Rendus de l'Acade mie Des Sciences de Paris*, *309*(2), 95–101.

Bill, M., Bussy, E., Cosca, M. A., Masson, H., & Hunziker, J. C. (1997). High precision U-Pb and 40Ar/39Ar dating of an alpine ophiolite (gets nappe, French Alps). *Eclogae Geologicae Helvetiae*, *90*, 43–54.

Bourdelle, F., & Cathelineau, M. (2015). Low-temperature chlorite geothermometry: A graphical representation based on a T–R2+–Si diagram. *European Journal of Mineralogy*, *27*, 617–626.

Bousquet, R., Goffé, B., Vidal, O., Oberhaensli, R., & Patriat, M. (2002). The tectono-metamorphic history of the Valaisan domain from the Western to the Central Alps: New constraints on the evolution of the Alps. *Geological Society of America Bulletin*, *114*, 207–225.

Bousquet, R., Oberhaensli, R., Goffé, B., Wiederkehr, M., Koller, F., Schmid, S. M., Schuster, R., Engi, M., Berger, A., & Martinotti, G. (2008). Metamorphism of metasediments at the scale of an orogen: A key to the tertiary geodynamic evolution of the Alps. In S. Siegesmund & N. Froitzheim (Eds.), *Tectonic aspects of the alpine-Dinaride-Carpathian system* (Vol. 298, pp. 393–412). Geological Society, Special Publications.

Brunet, C., Monié, P., Jolivet, L., & Cadet, J. P. (2000). Migration of compression and extension in the Tyrrhenian Sea, insights from $^{40}Ar/^{39}Ar$ ages on micas along a transect from Corsica to Tuscany. *Tectonophysics*, *321*, 127–155.

Cabanis, B., Cochemé, J. J., Vellutini, P. J., Joron, J. L., & Treuil, M. (1990). Post- collisional Permian volcanism in northwestern Corsica: An assessment based on mineralogy and trace-element geochemistry. *Journal of Volcanology and Geothermal Research*, *44*, 51–67.

Cathelineau, M. (1988). Cation site occupancy in chlorites and illites as a function of temperature. *Clay Minerals*, *23*, 471–485.

Cathelineau, M., & Nieva, D. (1985). A chlorite solid solution geothermometer the los Azufres (Mexico) geothermal system. *Contributions to Mineralogy and Petrology*, *91*, 235–244.

Daniel, J. M., Jolivet, L., Goffé, B., & Poinssot, C. (1996). Crustal-scale strain partitioning: Footwall deformation below the alpine oligo-Miocene detachment of Corsica. *Journal of Structural Geology*, *18*(1), 41–59.

Danišik, M., Kuhlemann, J., Dunkl, I., Székely, B., & Frisch, W. (2007). Burial and exhumation of Corsica (France) in the light of fission track data. *Tectonics*, *26*, TC1001. https://doi.org/10.1029/2005TC001938

Di Rosa, M. (2021). *Tectono-metamorphic evolution of the continental units along the edge between alpine and Hercynian Corsica* (p. 222). Firenze University Press.

Di Rosa, M., De Giorgi, A., Marroni, M., & Pandolfi, L. (2017). Geology of the area between Golo and Tavignano valleys (Central Corsica): A snapshot of the continental metamorphic units of alpine Corsica. *Journal of Maps*, *13*, 644–653.

Di Rosa, M., De Giorgi, A., Marroni, M., & Vidal, O. (2017). Syn-convergence exhumation of continental crust: Evidence from structural and metamorphic analysis of the Monte Cecu area, alpine Corsica (northern Corsica, France). *Geological Journal*, *52*, 919–937.

Di Rosa, M., Farina, F., Lanari, P., & Marroni, M. (2020). Pre-alpine thermal history recorded in the continental crust from alpine Corsica (France):

Evidence from zircon and allanite LA-ICP-MS dating. *Swiss Journal of Geosciences*, *113*, 19.

Di Rosa, M., Frassi, C., Malasoma, A., Marroni, M., Meneghini, F., & Pandolfi, L. (2020). Syn-exhumation coupling of oceanic and continental units along the western edge of the alpine Corsica: A review. *Ofioliti*, *45*(2), 71–102.

Di Rosa, M., Frassi, C., Marroni, M., Meneghini, F., & Pandolfi, L. (2020). Did the "autochthonous" European foreland of Corsica Island (France) experience alpine subduction? *Terra Nova*, *32*, 34–43.

Di Rosa, M., Frassi, C., Meneghini, F., Marroni, M., Pandolfi, L., & De Giorgi, A. (2019). Tectono-metamorphic evolution in the European continental margin involved in the alpine subduction: New insights from the alpine Corsica, France. *Comptes Rendus de Académié de Sciences Paris*, *351*(5), 384–394.

Di Rosa, M., Meneghini, F., Marroni, M., Frassi, C., & Pandolfi, L. (2020). The coupling of high-pressure oceanic and continental units in alpine Corsica: Evidence for syn-exhumation tectonic erosion at the roof of the plate interface. *Lithos*, *354-355*, 105328.

Di Rosa, M., Meneghini, F., Marroni, M., Hobbs, N., & Vidal, O. (2019). The exhumation of continental crust in collisional belts: Insights from the deep structure of alpine Corsica in the Cima Pedani area. *Journal of Geology*, *127*(3), 263–288.

Di Vincenzo, G., Grande, A., Prosser, G., Cavazza, W., & DeCelles, P. G. (2016). $^{40}Ar/^{39}Ar$ laser dating of ductile shear zones from Central Corsica (France): Evidence of alpine (middle to late Eocene) syn-burial shearing in *Variscan granitoids*. *Lithos*, *262*, 369–383.

Dubacq, B., Vidal, O., & De Andrade, V. (2010). Dehydration of dioctahedral aluminous phyllosilicates: Thermodynamic modelling and implications for thermobarometric estimates. *Contributions to Mineralogy and Petrology*, *159*, 159–174.

Durand-Delga, M. (1984). Principaux traits de la Corse Alpine et correlations avec les Alpes Ligures. *Memorie Della Societa Geologica Italiana*, *28*, 285–329.

Durand-Delga, M., Peybernès, B., & Rossi, P. (1997). Arguments en faveur de la position, au Jurassique, des ophiolites de Balagne (Haute-Corse, France) au voisinage de la marge continentale européenne. *Comptes Rendus de l'Académie Des Sciences*, *325*, 973–981.

Elter, P., & Pertusati, P. (1973). Considerazioni sul limite Alpi-Appennino e sulle relazioni con l'arco delle Alpi Occidentali. *Memorie Della Societa Geologica Italiana*, *12*, 359–375.

Favre, P., & Stampfli, G. M. (1992). From rifting to passive margin: The example of the Red Sea, Central Atlantic and alpine Tethys. *Tectonophysics*, *215*, 69–97.

Ferrandini, J., Ferrandini, M., Rossi, P., & Savary-Sismondini, B. (2010). Définition et datation de la formation de Venaco (Corse): dépot d'origine gravitaire d'age Priabonien. *Comptes Rendus de Geoscience*, *342*, 921–929.

Ferrandini, M., Ferrandini, J., Loye-Pilot, M. D., Butterlin, J., Cravatte, J., & Janin, M. C. (1998). Le Miocène du bassin de Saint-Florent (Corse): modalités de la transgression du Burdigalien supérieur et mise en évidence du Serravallien. *Geobios*, *31*(1), 125–137.

Fournier, M., Jolivet, L., Goffé, B., & Dubois, R. (1991). The alpine Corsica metamorphic core complex. *Tectonics*, *10*, 1173–1186.

Frassi, C., Di Rosa, M., Farina, F., Pandolfi, L., & Marroni, M. (2022). Anatomy of a deformed upper crust fragment from western alpine Corsica (France): Insights into continental subduction processes. *International Geology Review*, *65*, 40–60. https://doi.org/10.1080/00206814.2022.2031315

Froitzheim, N., & Manatchal, G. (1996). Kinematics of Jurassic rifting, mantle exhumation, passive margin formation in the Austroalpine and Penninic nappes (eastern Switzerland). *Geological Society Annual Bulletin*, *108*, 1120–1333.

Garfagnoli, F., Menna, F., Pandeli, E., & Principi, G. (2009). Alpine metamorphic and tectonic evolution of the Inzecca-Ghisoni area (southern alpine Corsica, France). *Geological Journal*, *44*, 191–210.

Gibbons, W., & Horak, J. (1984). Alpine metamorphism of Hercynian hornblende granodiorite beneath the blueschist facies Schistes Lustrés nappe of NE Corsica. *Journal of Metamorphic Geology*, *2*, 95–113.

Gueydan, F., Leroy, Y. M., Jolivet, L., & Agard, P. (2003). Analyses of continental midcrustal strain localization induced by microfaultinf and reactionsoftening. *Journal of Geophysical Research*, *108*, 2064–2081.

Guieu, G., Loye-Pilot, M. D., Lahondére, D., & Ferrandini, J. (1994). *Carte géologique de France (1/50000), feuille Bastia (1111)*. BRGM.

Handy, M. R., Schmid, S. M., Bousquet, R., Kissling, E., & Bernoulli, D. (2010). Reconciling plate–tectonic reconstructions of alpine Tethys with the geological–geophysical record of spreading and subduction in the Alps. *Earth-Science Reviews*, *102*, 121–158.

Inoue, A., Kurokawa, K., & Hatta, T. (2009). Application of chlorite Geothermometry to hydrothermal alteration in Toyoha geothermal system, southwestern Hokkaido, Japan. *Resource Geology*, *60*(1), 52–70.

Jakni, B., Poupeau, G., Sosson, M., Rossi, P., Ferrandini, J., & Guennoc, P. (2000). Dénudations cénozoiques en Corse: une analyse thermochronologique par traces de fission sur apatites. *Comptes Rendus de Académié de Sciences Paris*, *331*, 775–782.

Jolivet, L., Daniel, J. M., & Fournier, M. (1991). Geometry and kinematics of ductile extension in alpine Corsica. *Earth and Planetary Science Letters*, *104*, 278–291.

Jolivet, L., Dubois, R., Fournier, M., Goffé, B., Michard, A., & Jourdan, C. (1990). Ductile extension in alpine Corsica. *Geology*, *18*, 1007–1010.

Jourdan, F., & Renne, P. R. (2007). Age calibration of the fish canyon sanidine $^{40}Ar/^{39}Ar$ dating standard using primary K-Ar standards. *Geochimica et Cosmochimica Acta*, *71*, 387–402.

Koppers, A. A. P. (2002). ArArCALC-software for $^{40}Ar/^{39}Ar$ age calculations. *Computers and Geosciences*, *28*(5), 605–619.

Lacombe, O., & Jolivet, L. (2005). Structural and kinematic relationships between Corsica and the Pyreneeses-Provence domain at the time of the Pyrenean orogeny. *Tectonics*, *24*, TC1003. https://doi.org/10.1029/2004TC001673

Lagabrielle, Y., & Polino, R. (1988). Un schéma structural du domaine des Schistes Lustrés ophiolitiféres au nord-ouest du massif du mont Viso (Alpes sudoccidentales) et ses implications. *Comptes Rendus de Académié de Sciences Paris*, *323*, 957–964.

Lahondère, D., & Guerrot, C. (1997). Datation Sm-Nd du métamorphisme éclogitique en Corse alpine: un argument pour l'existence au Crétacé supérieur d'une zone de subduction active localisée sous le bloc corso-sarde. *Géologie de France*, *3*, 3–11.

Lanari, P. (2012). *Micro-cartgraphie P-T- dans les roches metamorphiques. Applications aux Alpes et à l'Himalaya*, (doctoral dissertation). Université de Grenoble.

Laporte, D., Fernandez, A., & Orsini, J. B. (1991). Le complexe d'île Rousse, Balagne, Corse du Nord-Ouest: pétrologie et cadre de mise en place des granitoïdes magnésiopotassiques. *Géologie de France*, *4*, 15–30.

Lardeaux, J. M., & Spalla, M. I. (1991). From granulites to eclogites in the Sesia zone (Italian Western Alps)—A record of the opening and closure of the Piedmont Ocean. *Journal of Metamorphic Geology*, *9*(1), 35–59.

Law, R. D. (2014). Deformation thermometry based on quartz crystal fabrics and recrystallization microstructures: A review. *Journal of Structural Geology*, *66*, 129–161.

Lee, J.-Y., Marti, K., Severinghaus, J. P., Kawamura, K., Yoo, H.-S., Lee, J. B., & Kim, J. S. (2006). A redetermination of the isotopic abundances of atmospheric Ar. *Geochimica et Cosmochimica Acta*, *70*, 4507–4512.

Levi, N., Malasoma, A., Marroni, M., Pandolfi, L., & Paperini, M. (2007). Tectono- metamorphic history of the ophiolitic lento unit (northern Corsica): Evidences for the complexity of accretion-exhumation processes in a fossil subduction system. *Geodinamica Acta*, *20*(1), 99–118.

Maggi, M., Rossetti, F., Corfu, F., Theye, T., Andersen, T. B., & Faccenna, C. (2012). Clinopyroxene-rutile phyllonites from east Tenda shear zone (alpine Corsica, France): Pressure-temperature-time constraints to the

alpine reworking of Variscan Corsica. *Journal of the Geological Society of London*, *169*, 723–732.

Malasoma, A., & Marroni, M. (2007). HP/LT metamorphism in the Volparone breccia (northern Corsica, France): Evidence for involvement of the Europe/Corsica continental margin in the alpine subduction zone. *Journal of Metamorphic Geology*, *25*, 529–545.

Malasoma, A., Marroni, M., Musumeci, G., & Pandolfi, L. (2006). High pressure mineral assemblage in granitic rocks from continental units, alpine Corsica, France. *Geological Journal*, *41*, 49–59.

Malasoma, A., Morelli, G., Di Rosa, M., Marroni, M., Pandeli, E., Principi, G., & Pandolfi, L. (2020). The stratigraphic and structural setting of metamorphic continental units from alpine Corsica: Clues from the area between Asco and Golo valleys (Central Corsica, France). *Journal of Maps*, *16*(2), 313–323.

Malavieille, J., Chemenda, A., & Larroque, C. (1998). Evolutionary model for the alpine Corsica: Mechanism for ophiolite emplacement and exhumation of high-pressure rocks. *Terra Nova*, *10*, 317–322.

Maluski, H. (1977). *Application de la méthode 40Ar/39Ar aux minéraux des roches cristallines perturbées par des événements thermiques et tectoniques en Corse*. Ph.D, (doctoral dissertation). Université de Montpellier.

Maluski, H., Mattauer, M., & Matte, P. H. (1973). Sur la presence de decrochement alpins en Corse. *Comptes Rendus de Académié de Sciences Paris*, *276*, 709–712.

Manatschal, G. (1995). *Jurassic rifting and formation of a passive continental margin (Platta and err nappes, eastern Switzerland): Geometry, kinematics and geochemistry of fault rocks and comparison with Galicia margin*. (doctoral dissertation). Zurich Universitat.

Marroni, M. (1991). Deformation history of the Mt. Gottero unit (internal Ligurid units, northern Apennines). *Bollettino Della Società Geologica Italiana*, *110*(3–4), 727–736.

Marroni, M., Meneghini, F., & Pandolfi, L. (2017). A revised subduction inception model to explain the late cretaceous, double Vergent orogen in the Precollisional Western Tethys: Evidence from the northern Apennines. *Tectonics*, *36*, 2227–2249.

Marroni, M., & Pandolfi, L. (2003). Deformation history of the ophiolite sequence from the Balagne nappe, northern Corsica: Insights in the tectonic evolution of the alpine Corsica. *Geological Journal*, *38*, 67–83.

Marroni, M., & Pandolfi, L. (2007). The architecture of an incipient oceanic basin: A tentative reconstruction of the Jurassic Liguria-Piemonte basin along the northern Apennine-alpine Corsica transect. *International Journal of Earth Sciences*, *96*, 1059–1078.

Martin, A. J., Rubatto, D., Vitale Brovarone, A., & Hermann, J. (2011). Late Eocene lawsonite-eclogite facies metasomatism of a granulite sliver associated to ophiolites in alpine Corsica. *Lithos*, *125*, 620–640.

Massonne, H. J., & Schreyer, W. (1987). Phengite geobarometry based on the limiting assemblage with K-feldspar, phlogopite, and quartz. *Contributions to Mineralogy and Petrology*, *96*, 212–224.

Mattauer, M., Faure, M., & Malavieille, J. (1981). Transverse lineation and large- scale structures related to alpine obduction in Corsica. *Journal of Structural Geology*, *3*(4), 401–409.

Mattauer, M., & Proust, F. (1976). La Corse alpine: un modèle de genès du metamorphisme haute pression par subdutcion de croute continentale sous du matériel océanique. *Comptes Rendus de Académié de Sciences Paris*, *282*, 1249–1251.

Meneghini, F., Pandolfi, L., & Marroni, M. (2020). Recycling of heterogeneous material in the subduction factory: Evidence from the sedimentary mélange of the internal Ligurian units, Italy. *Journal of the Geological Society*, *177*, 587–599.

Ménot, R. P., & Orsini, J. B. (1990). Evolution du socle anté-stéphanien de Corse: événements magmatiques et métamorphiques. *Schweizerische Mineraogische Und Petrographische Mittelungen*, *70*, 35–53.

Meresse, F., Lagabrielle, Y., Malavieille, J., & Ildefonse, B. (2012). A fossil ocean- continent transition of the Mesozoic Tethys preserved in the Schistes Lustrés nappe of northern Corsica. *Tectonophysics*, *579*, 4–16.

Michard, A., & Martinotti, G. (2002). The Eocene unconformity of the Brianconnais domain in the French-Italian Alps, revisited (Marguareis massif, Cuneo); a hint for a late cretaceous-middle Eocene frontal bulge setting. *Geodinamica Acta*, *15*, 289–301.

Molli, G. (2008). Northern Apennine-Corsica orogenic system: An updated overview. In S. Siegesmund, B. Fugenschuh, & N. Froitzheim (Eds.), *Tectonic aspects of the alpine-Dinaride-Carpathian system* (Vol. 298, pp. 413–442). Geological Society of London Special Publication.

Molli, G., & Malavieille, J. (2011). Orogenic processes and the Corsica/Apennines geodynamic evolution: Insights from Taiwan. *International Journal of Earth Sciences*, *100*(5), 1207–1224.

Molli, G., & Tribuzio, R. (2004). Shear zones and metamorphic signature of subducted continental crust as tracers of the evolution of the Corsica/northern Apennine orogenic system. In G. I. Alsop, R. E. Holdsworth, K. J. W. McCaffrey, & M. Handy (Eds.), *Flow processes in faults and shear zones* (Vol. 224, pp. 321–335). Geological Society of London Special Publications.

Molli, G., Tribuzio, R., & Marquer, D. (2006). Deformation and metamorphism at the eastern border of Tenda massif (NE Corsica): A record of subduction and exhumation of continental crust. *Journal of Structural Geology*, *28*, 1748–1766.

Pandolfi, L., Marroni, M., & Malasoma, A. (2016). Stratigraphic and structural features of the bas-Ostriconi unit (Corsica): Paleogeographic implications. *Comptes Rendus de Académié de Sciences Paris*, *348*, 630–640.

Paquette, J. L., Ménot, R. P., Pin, C., & Orsini, J. B. (2003). Episodic and short-lived granitic pulses in a post-collisional setting: Evidence from precise U-Pb zircon dating through a crustal cross-section in Corsica. *Chemical Geology*, *198*, 1–20.

Passchier, C. W., & Trouw, R. A. J. (2005). *Microtectonics* (Vol. 16). Springer.

Ramsay, J. G. (1967). *Folding and fracturing of rocks*. McGraw-Hill.

Ravna, E. J. K., Andersen, T. B., Jolivet, L., & De Capitani, C. (2010). Cold subduction and the formation of lawsonite-eclogite from prograde evolution of eclogitized pillow lava from Corsica. *Journal of Metamorphic Geology*, *28*, 381–395.

Rossetti, F., Cavazza, W., Di Vincenzo, G., Lucci, F., & Theye, T. (2022). Alpine tectono-metamorphic evolution of the Corsica basement. *Journal of Metamorphic Geology*, *41*(2), 299–326. https://doi.org/10.1002/jmg.12696

Rossetti, F., Glodny, J., Theye, T., & Maggi, M. (2015). Pressure temperature deformation- time of the ductile alpine shearing in Corsica from orogenic construction to collapse. *Lithos*, *218-219*, 99–116.

Rossi, P., Cocherie, A., & Fanning, M. (2015). Evidence in Variscan Corsica of a brief and voluminous late carboniferous to early Permian volcanic-plutonic event contemporaneous with a high-temperature/low-pressure metamorphic peak in the lower crust. *Bulletin de la Société Géologique de France*, *186*(2–3), 171–192.

Rossi, P., Durand-Delga, M., Caron, J. M., Guieu, G., Conchon, O., Libourel, G., & Loye-Pilot, M. (1994). Carte Geologique de la France, feuille Corte (1110). BRGM, Orléans, scale 1:50000, 1 sheet.

Rossi, P., Oggiano, G., & Cocherie, A. (2009). A restored section of the "southern Variscan realm" the Corsica–Sardinia microcontinent. *Comptes Rendus Geosciences*, *341*, 224–238.

Saccani, E., Padoa, E., & Tassinari, R. (2000). Preliminary data on the Pineto gabbroic massif and Nebbio basalts: Progress toward the geochemical characterization of alpine Corsica ophiolites. *Ofioliti*, *25*, 75–86.

Schmid, S. M., Pfiffner, O. A., Froitzheim, N., Schönborn, G., & Kissling, E. (1996). Geophysical–geological transect and tectonic evolution of the swiss–Italian Alps. *Tectonics*, *15*(5), 1036–1064.

Spear, F. S. (1993). The metamorphism of mafic rocks. *Metamorphic phase Equilibria and Pressure-Temperature-Time paths*, *Mineralogical Society of America*.

Steiger, R. H., & Jäger, E. (1977). Subcommission on geochronology: Convention on the use of decay constants in geo- and cosmochronology. *Earth and Planetary Science Letters*, *36*, 359–362.

Stipp, M., Stunitz, H., Heilbronner, R., & Schmid, S. M. (2002). Dynamic recrystallization of quartz: Correlation between natural and experimental conditions. *Geological Society London Special Publications*, *200*, 171–190. https://doi.org/10.1144/GSL.SP.2001.200.01.11

Tribuzio, R., & Giacomini, F. (2002). Blueschist facies metamorphism of peralkaline rhyolites from Tenda crystalline massif (northern Corsica): Evidence for involvement in the alpine subduction event? *Journal of Metamorphic Geology*, *20*, 513–526.

Vidal, O., & Parra, T. (2000). Exhumation paths of high-pressure metapelites obtained from local equilibria for chlorite–phengite assemblage. *Geological Journal*, *35*, 139–161.

Vitale Brovarone, A., Beyssac, O., Malavieille, J., Molli, G., Beltrando, M., & Compagnoni, R. (2012). Stacking and metamorphism of continuous segments of subducted lithosphere in a high-pressure wedge: The example of alpine Corsica (France). *Earth-Science Reviews*, *116*, 35–56.

Vitale Brovarone, A., & Herwartz, D. (2013). Timing of HP metamorphism in the Schistes Lustrés of alpine Corsica: New Lu-Hf garnet and lawsonite ages. *Lithos*, *172-173*, 175–191.

Warburton, J. (1986). The ophiolite-bearing Schistes Lustrés nappe in alpine Corsica: A model for the implacement of ophiolites that have suffered HP/LT metamorphism. *Geological Society of America Bulletin Memoirs*, *164*, 313–331.

Waters, C. N. (1990). The Cenozoic tectonic evolution of alpine Corsica. *Journal of Geological Society of London*, *147*, 811–824.

Zarki-Jakni, B., Van Der Beek, P., Poupeau, G., Sosson, M., Labrin, E., Rossi, P., & Ferrandini, J. (2004). Cenozoic denudation of Corsica in response to Ligurian and Tyrrhenian extension: Results from apatite fission track thermochronology. *Tectonics*, *23*, TC1003. https://doi.org/10.1029/2003TC001535

SUPPORTING INFORMATION

Additional supporting information can be found online in the Supporting Information section at the end of this article.

How to cite this article: Di Rosa, M., Sanità, E., Frassi, C., Lardeaux, J. M., Corsini, M., Marroni, M., & Pandolfi, L. (2023). A journey of the continental crust to and from mantle depth: The *P–T–t-d* path of Venaco unit, Alpine Corsica (France). *Geological Journal*, 1–19. https://doi.org/10.1002/gj.4872